Designing Composite Triangular Subdivision Schemes

Peter Oswald

Bell Laboratories, Lucent Technologies
600 Mountain Avenue
Murray Hill, NJ 07974
e-mail: poswald@research.bell-labs.com

Abstract

The paper iterates on the observation made independently by several groups of authors that building subdivision schemes out of simple, very local and geometrically invariant averaging rules is convenient both from a theoretical and practical point of view. We review the benefits of this approach with special emphasis on the smoothness analysis of the limit surfaces, derive certain guidelines for how to design reasonable composite schemes, and apply those to hex-by-seven subdivision.

1 Introduction

Recently, there has been considerable interest in the classification of subdivision schemes, on the one hand, and in building a unified theory for the various existing variants of topology refinement and subdivision, on the other. A common theme in these investigations is that everything in subdivision is built upon a few primitives. E.g., the way the new mesh topology is defined through elementary polyhedral operators seems crucial, and suggests some very simple averaging operators and lower-order basic subdivision schemes (see [21, 25], and [12, 13]). More general basic averaging rules for triangular meshes are considered in [27]. Data structures (mostly face-based and edge-based, see [1]) also influence what could be considered as the most basic schemes. The other common thread is the realization that repeating simple rules is a convenient way to create families of higher-order subdivision schemes (the classification into lower- and higher-order has no precise meaning but can be loosely associated with higher approximation/smoothness order resp. larger stencil size), and may replace the tedious task of finding good higher-order schemes in an ad hoc fashion, especially if they are supposed to work on irregular meshes, too.

Our angle here is to outline a design approach for families of composite triangular subdivision schemes that includes their smoothness analysis as an integral part. It summarizes the observations made in [27, 19], where specifically $\sqrt{3}-$subdivision schemes have been treated. Similar results have appeared in many other sources, for various

types of refinement. The approach covers hexagonal subdivision as well which is the face-based counterpart of vertex-based triangular subdivision. As a special example, we consider $\sqrt{7}$-subdivision schemes which in their face-based, i.e., hexagonal interpretation have appeared in connection with pyramid schemes for modeling the function of the retina [32, 24] resp. for representing terrain data in geophysical applications [28].

Besides the restriction on triangles, we will always neglect boundaries (i.e., assume that the triangular complex representing the mesh has no boundary edges), and assume that in the topology refinement step the old vertex set is a subset of the new one. This excludes some of the dual and mixed schemes discussed in [12] and also many of the meta-schemes proposed in [21, 25] but still includes the most common primal and dual subdivision schemes on triangular meshes with different dilation factors. Quadrilateral topologies are easier to deal with. Mixed topologies (say, mixtures of quads and triangles that will not disappear given certain topology refinement rules) are not considered here, their smoothness analysis is slightly more complicated, see [22]. We would also like to mention that, with the exception of some lower-order, not very useful examples, the composition rules advocated here do not naturally result in interpolatory subdivision schemes, and thus are not recommended for generating those.

The material is grouped into 3 sections. In Section 2 we introduce basic terminology and some examples. The guidelines for constructing higher-order composite schemes are collected and partly motivated by simplifications in their analysis in Section 3. In the final Section 4 the design rules are applied to construct hex-by-seven subdivision schemes.

2 Terminology and Examples

We will take the more traditional approach of introducing subdivision schemes by describing the topology refinement rules (connectivity of the triangular mesh) and the geometry refinement (local averaging rules to position the geometric elements in $\mathbb{R}^3$) separately.

In its face-based representation, a *triangular mesh topology* $\mathcal{T} := (\mathcal{V}, \mathcal{F})$ is given by a vertex set $\mathcal{V}$ (normally a list of integers) and a face set $\mathcal{F} \subset \mathcal{V} \times \mathcal{V} \times \mathcal{V}$. If $f = (v_1, v_2, v_3) \in \mathcal{F}$ then the 3 vertices v_i must be pairwise different, and are called the vertices of f (for short, $v_i \subset f$). Similarly, $e_1 = (v_1, v_2)$, $e_2 = (v_2, v_3)$, $e_3 = (v_3, v_1)$ are called the edges of f ($e_i \subset f$), and we will denote the set of all such edges by $\mathcal{E} \subset \mathcal{V} \times \mathcal{V}$. For the moment being edges are considered to have no orientation, and we will identify the edges (v, v') and (v', v). Similarly, two faces are the same if their vertex sets are identical (the order of the vertex triple does not matter). The basic compatibility condition (which also implies that there is no boundary) is that for any face f and any of its edges $e \subset f$, there is exactly one face $f' \neq f$ such that $e \subset f'$ (we call e the common edge of f and f'). Finally, we assume that the valence $k := k(v)$, i.e., the number of different faces f attached to a vertex v ($v \subset f$), is always finite but at least 3. Thus, each vertex $v \in \mathcal{V}$ has a natural *vertex* or 1-*ring neighborhood* $N(v)$ containing k vertices v_i, k faces $f_i = (v, v_i, v_{i+1})$, and k edges $e_i = (v, v_i) = f_i \cap f_{i-1}$

($v_{k+1} = v_1,\ f_0 = f_k$) attached to it. Similarly, each face $f \in \mathcal{F}$ has a natural *face* or *flap neighborhood* $N(f)$ containing 3 more faces f_i besides f, and 3 vertices v_i and edges e_i directly attached to it. There is also a basic *edge neighborhood* $N(e)$ consisting of the two faces f_1 and f_2 that share this edge, its two endpoint vertices v_i, and 4 more edges e_i. These neighborhoods are easily accessible through the basic geometric data structures. Figure 1 illustrates them. Note finally that, instead of choosing $\mathcal{V}, \mathcal{F}$ as the primary entities and deriving the edge set $\mathcal{E}$ from them, we could also declare $\mathcal{V}$, $\mathcal{E}$ as primary, and define the face set $\mathcal{F}$ from them. This is related to edge-based data structures (see [1] for some motivation) but will not be pursued here.

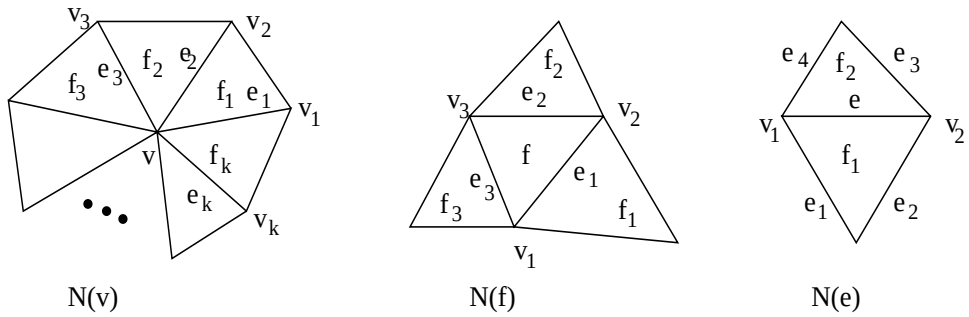


Figure 1: Basic vertex, face, and edge neighborhoods in triangular mesh topologies

General *polygonal mesh topologies* are defined in the same way, with the exception that faces are defined as $n(f)$-tuples, i.e., have $n(f)$ edges and vertices, where $n(f) \geq 3$ is finite and may change from face to face. As a consequence, the above described neighborhoods may become much more complicated. An example is the dual $\mathcal{T}^* = (\mathcal{V}^*, \mathcal{F}^*)$ of a triangular mesh topology $\mathcal{T}$ which is obtained by identifying $\mathcal{V}^* := \mathcal{F}$ and $\mathcal{F}^* \cong \mathcal{V}$ in the sense that the face f^* associated with $v \in \mathcal{V}$ is given by the $k(v)$-tuple $(v_1^*, \ldots, v_{k(v)}^*) \equiv (f_1, \ldots, f_{k(v)})$. Since $n(f) \equiv 3$ for the original triangular mesh topology $\mathcal{T}$, we have $k(v^*) \equiv 3$ for all $v^* \in \mathcal{V}^*$ while $n(f^*) = k(v)$ becomes variable. Figure 2 shows portions of $\mathcal{T}$ and its dual $\mathcal{T}^*$. Since often the majority of vertices in a triangular topology has valence 6, the dual $\mathcal{T}^*$ is also referred to as *hexagonal mesh topology*.

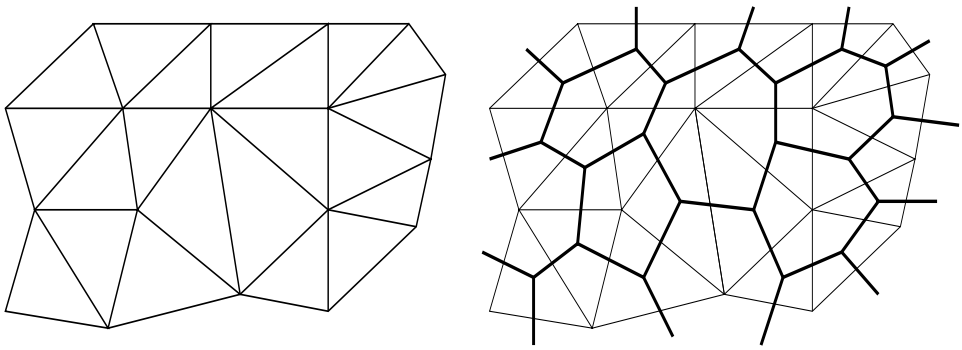


Figure 2: a) Triangular $\mathcal{T}$ and b) its dual $\mathcal{T}^*$ (or hexagonal) mesh topologies

The *topology refinement* is a procedure

$$TR: \qquad \mathcal{T} = (\mathcal{V}, \mathcal{F}) \quad \longmapsto \quad \mathcal{T}' = (\mathcal{V}', \mathcal{F}'),$$

applicable to an arbitrary triangular mesh topology $\mathcal{T}$. Usually, it is cast in geometric terms like vertex-, face-, or edge-splitting (see [33] for an example), and can be explained best on triangulations embedded into $\mathbb{R}^2$. A more systematic approach applicable to general mesh topologies is the representation of TR as a composition of a few elementary polyhedra operators [13] which is very close in spirit to our approach. Since we do not aim at utmost generality, we will just describe the assumptions on TR followed in this paper. First of all, we will always assume $\mathcal{V} \subset \mathcal{V}'$, and postulate that TR is *uniform* and *local*. This vaguely means that the new vertices/faces/edges are uniformly inserted into the old $\mathcal{T}$ (e.g., the number of vertices in $\mathcal{V}'$ belonging to a face (or edge) of $\mathcal{T}$ is constant and finite). In particular, the application of TR to a uniform 3-directional triangular mesh of $\mathbb{R}^2$ must lead to another, down-scaled by a factor $\sqrt{m}$, and possibly rotated uniform 3-directional triangular mesh, where $m > 1$ is an integer (called *dilation factor*). We will not formalize this assumption as it is usually clear from the context, or implemented by reverse engineering (i.e., by transfering the rules for TR from the uniform setting to arbitrary $\mathcal{T}$). Figure 3 a) shows the example of $\sqrt{3}$-refinement, where

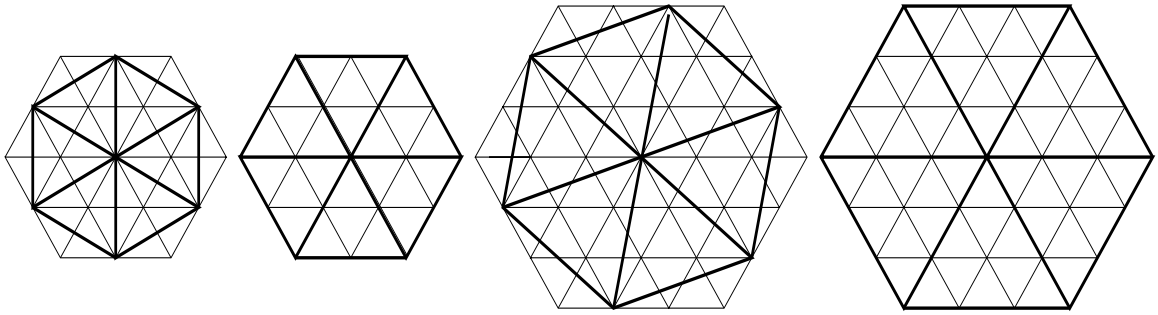


Figure 3: The triangular TR with $m \leq 9$ in the uniform setting

the geometric rule underlying TR is the insertion of one new vertex (the barycenter) per face, and creating $\mathcal{F}'$ as the set of all triangles with one old vertex v and two new vertices v_1, v_2 such that the latter are the barycenters of two faces sharing a common edge with endpoint v. Following [24] or [12], it is easy to find all theoretically possible scaling factors $\sqrt{m}$ under these assumptions (following [24] or [12]), they are given by the formula

$$m = k^2 - kl + l^2, \qquad l = 0, 1, \ldots, [k/2], \;\; k \geq 2,$$

and can be found from the fact that all possible embeddings of a uniform 3-directional triangular mesh into another one are (up to symmetry and shift transformations) described by an edge of length $\sqrt{m}$ connecting two vertices of the finer triangulation. Figure 3 b)-d) shows these embeddings for some more values of m. Note that for $m \leq 48$ and

up to symmetry transformations, the uniform TR for triangular mesh topologies with $\mathcal{V} \subset \mathcal{V}'$ are uniquely determined by the dilation factor m, however, one has to be careful with choosing the representer TR consistently, to use the analysis tools explained in Section 4 correctly (we come back to this in Section 4).

Only the smaller values $m = 3$ (barycenter insertion), $m = 4$ (quadrisection or edge midpoint insertion, this is the most widely used case), and $m = 7$ [32, 24, 28] are probably of practical interest since the storage associated with $\mathcal{T}$ grows as $\sim m^j$ with the number of refinement steps j. However, if subdivision is performed as part of an adaptive pyramid transform larger values of m might provide fast zoom-in features, see [24] for an example with $m = 19$. Our assumptions exclude values such as $m = 2$ (quincunx schemes) or $m = 5$ which can only be realized in quadrilateral mesh topologies resp. in schemes where the condition $\mathcal{V} \subset \mathcal{V}'$ is relaxed (see [5] for an example).

The description of the mesh topology is complemented by an embedding of $\mathcal{T}$ into $\mathbb{R}^3$ (or $\mathbb{R}^n$ for that matter) which allows us to interpret the mesh as a discrete surface in space. Generally, the embedding σ can be *vertex-based*

$$\sigma_{\mathcal{V}} : \quad \mathcal{V} \quad \longmapsto \quad \mathbb{R}^3,$$

or *face-based*

$$\sigma_{\mathcal{F}} : \quad \mathcal{F} \quad \longmapsto \quad \mathbb{R}^3,$$

or *edge-based*

$$\sigma_{\mathcal{E}} : \quad \mathcal{F} \quad \longmapsto \quad \mathbb{R}^3,$$

or *mixed*, i.e., a collection of several such mappings. E.g., the point set $\sigma_{\mathcal{V}}(\mathcal{V})$ yields a triangulated surface in $\mathbb{R}^3$ after local linear interpolation w.r.t. each triangle of $\mathcal{F}$ is performed (triangulated surfaces can be associated with $\sigma_{\mathcal{F}}$ and $\sigma_{\mathcal{E}}$ in various ways, too, but we will not dwell on these irrelevant details). Similarly, the topology refinement TR needs to be complemented by a *geometry refinement operator* GR which describes the way the embedding for the refined mesh topology $\mathcal{T}'$ is obtained from the one for $\mathcal{T}$. The most popular cases are *vertex-based* GR mapping $\sigma_{\mathcal{V}}$ into $\sigma_{\mathcal{V}'}$ (often called *primal subdivision schemes*), and *face-based* GR mapping $\sigma_{\mathcal{F}}$ into $\sigma_{\mathcal{F}'}$ (also called *dual subdivision schemes*). This terminology is natural since a face(vertex)-based GR on $\mathcal{T}$ can be interpreted as vertex(face)-based GR on the dual $\mathcal{T}^*$ vice versa. In particular, any vertex-based subdivision scheme for hexagonal mesh topologies is equivalent to a face-based subdivision scheme on the dual triangular mesh topologies, and there is no need to do a separate analysis for hexagonal meshes, if face- and vertex-based schemes are studied in the triangular case. Edge-based GR have not been studied explicitly in connection with geometric modeling although they come up implicitly in the form of prolongation operators for multigrid solvers for certain elliptic systems of PDE such as Stokes or Maxwell equations. We do not consider Hermite GR [10], where not only point positions but also gradient (or even curvature) information is prescribed by the mapping σ.

Typically, a GR must be linear, local, and geometrically invariant. One way to achieve this is to describe the GR by local, geometrically invariant *coefficient stencils*.

E.g., for a vertex-based scheme, the stencil associates with each $v' \in \mathcal{V}'$ a geometrically invariant neighborhood $N_{GR}(v') \subset \mathcal{V}$ and a weight function $w : N_{GR}(v') \to \mathbb{R}$, and defines the linear GR operation as follows:

$$\sigma_{\mathcal{V}'}(v') = \sum_{v \in N_{GR}(v')} w(v)\sigma_{\mathcal{V}}(v), \qquad 1 = \sum_{v \in N_{GR}(v')} w(v). \tag{1}$$

The neighborhood must not depend on the location of v' in $\mathcal{V}'$ but only on the type of v' which is determined by the corresponding TR. The weight normalization condition stated in (1) will always be assumed. In particular, for $\sqrt{3}$-refinement there are 2 stencils (one for old vertices, i.e., vertices from $\mathcal{V}' \cap \mathcal{V}$, and one for the newly inserted vertices, i.e., the barycenters of old faces), and we show the geometrically sound weights for a possible geometrically invariant neighborhood $N_{GR}(v')$ in Fig. 4 a). Similar conventions are used for other types of GR, examples of stencils for a face-based GR and 2-refinement are shown in Fig. 4 b).

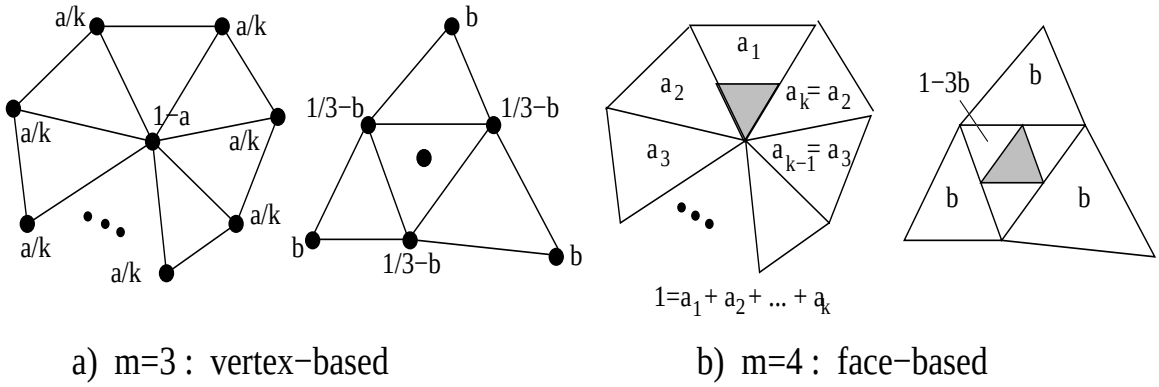


Figure 4: GR families: a) vertex-based, $m = 3$ (see [19]), and b) face-based, $m = 4$

Although this approach is general, it becomes cumbersome for larger m resp. stencil sizes. It also introduces a lot of free parameters which need to be determined in the course of the analysis of a scheme. Since the type of $v' \in \mathcal{V}'$ depends on the chosen TR, a lot of different situations have to be considered. For regular mesh topologies, this can be handled [8] by directly working with the mask coefficients of the associated refinement equation, and describing the geometric symmetry constraints by an associated group of symmetry transformations (see Section 3.1 for more details). An alternative [27] is to construct stencils and stencil families by composing a few basic operations: A simple stencil for GR followed (and possibly preceded) by averaging rules that are applicable not only on regular mesh topologies. A *triangular averaging rule* AR is similar to a GR, with the only difference that it transforms an embedding σ associated with $\mathcal{T}$ into a new one for the same $\mathcal{T}$. For simplicity, only AR which map σ_X into σ_Y are considered, where X, Y are place-holders for $\mathcal{V}, \mathcal{F}, \mathcal{E}$, respectively. They can be described again by coefficient stencils, i.e., by geometrically invariant neighborhoods of vertices, faces, edges associated with $\mathcal{T}$ (not with $\mathcal{T}'$) as shown in Fig. 1 and weight functions on them. To have enough flexibility, we fix a *basic* AR for each X, Y combination, and denote it for

our convenience by $Y \overset{c}{\leftarrow} X$, where the parameter c is present only if $X = Y$. This gives the 9 stencils depicted in Fig. 5, where $k = k(v)$ denotes the valence of the center vertex v. Some special cases of the parametric $X \overset{c}{\leftarrow} X$ rules are covered by composing certain

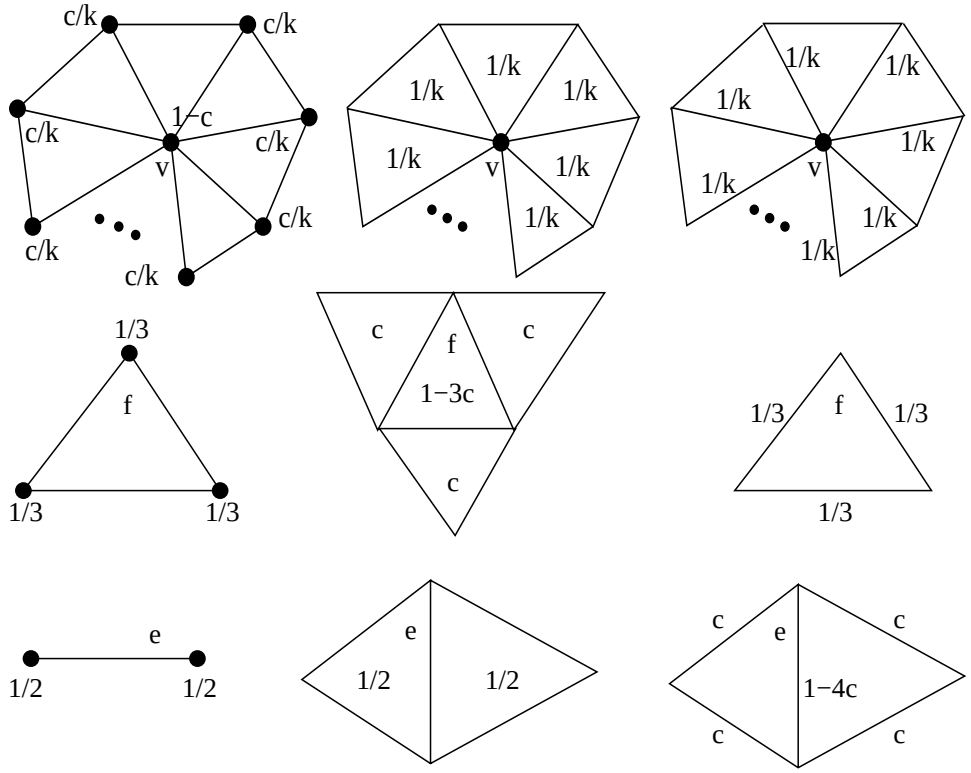


Figure 5: The 9 basic AR for obtaining v-values (top row), f-values (center) resp. e-values (bottom)

non-parametric $X \leftarrow Y$ rules ($X \neq Y$):

$$\mathcal{F} \overset{1/6}{\leftarrow} \mathcal{F} = \mathcal{F} \leftarrow \mathcal{E} \leftarrow \mathcal{F}, \qquad \mathcal{E} \overset{1/6}{\leftarrow} \mathcal{E} = \mathcal{E} \leftarrow \mathcal{F} \leftarrow \mathcal{E},$$

or

$$\mathcal{V} \overset{1/2}{\leftarrow} \mathcal{V} = \mathcal{V} \leftarrow \mathcal{E} \leftarrow \mathcal{V}, \qquad \mathcal{V} \overset{2/3}{\leftarrow} \mathcal{V} = \mathcal{V} \leftarrow \mathcal{F} \leftarrow \mathcal{V},$$

Also, since $\mathcal{F} \leftarrow \mathcal{V} = \mathcal{F} \leftarrow \mathcal{E} \leftarrow \mathcal{V}$, there is some redundancy in the above list. In the following we will only use the above basic AR to compose whatever subdivision scheme we want to achieve (later, in connection with the smoothness analysis for extraordinary vertices, we will modify some of these rules according to valence information).

Since all AR only act on one and the same triangular mesh topology $\mathcal{T}$, we need at least one GR that connects information on $\mathcal{T}$ to information on the refined mesh topology $\mathcal{T}'$. According to our assumptions, there is one GR which does not depend on the geometric details of the particular TR:

$$GR_m \ : \qquad \sigma_{\mathcal{V}} \quad \longmapsto \sigma_{\mathcal{V}'}(v') = \begin{cases} m\sigma_{\mathcal{V}}(v'), & v' \in \mathcal{V}, \\ 0, & v' \in \mathcal{V}' \backslash \mathcal{V}. \end{cases} \tag{2}$$

It involves only the dilation factor m, and is extremely simple in its implementation. Certainly, if the TR is fixed other simple GR might come to mind (however, there will be some benefits in the smoothness analysis if we stick to GR_m as the only candidate).

With all this terminology at hand, let us define a *composite subdivision operator* S (on triangular mesh topologies and for a TR with dilation factor m) by

$$S = AR'_{N_2} \circ \ldots \circ AR'_1 \circ GR_m \circ AR_{N_1} \circ \ldots \circ AR_1, \tag{3}$$

where $\{AR_n = X_n \overset{(c)}{\leftarrow} X_{n-1}\}$ is a collection of $N_1 \geq 0$ averaging rules acting on $\mathcal{T}$ such that $X_{N_1} = \mathcal{V}$, and $\{AR'_n = Y_n \overset{(c)}{\leftarrow} Y_{n-1}\}$ is a collection of $N_2 \geq 0$ averaging rules acting on $\mathcal{T}'$ such that $Y_0 = \mathcal{V}'$. Clearly, to be compatible with our above restrictions on the GR to be considered, we also assume that $Y_{N_2} = X'_0 := X'$. Finally, the *subdivision scheme* associated with S consists of applying S iteratively, starting from an initial triangular mesh topology $\mathcal{T}^0$ and embedding $\sigma^0 := \sigma_{X^0}$. This creates a sequence $\{(\mathcal{T}^j, \sigma^j)\}$, $j \geq 0$, where $\mathcal{T}^{j+1} = (\mathcal{T}^j)'$ is the result of applying TR, and $\sigma^{j+1} = S\sigma^j$. Since we apply the same TR and S for each j, the scheme is called *stationary*. The goal of the analysis of any such scheme is to make sure that the point sets given by σ^j (more precisely: the associated triangulated surfaces) converge to a limit surface $S^\infty\sigma^0$ of reasonable shape and smoothness properties for all reasonable initial configurations $(\mathcal{T}^0, \sigma^0)$.

This paper is about exploring the structure of composite subdivision operators S to simplify the smoothness analysis, which we will explain in the next section. Before going on, let us note some examples of triangular subdivision schemes that are covered by the approach. There are many others, especially for quadrilateral topologies.

- Loop's scheme [23] and its higher-order relatives for quadrisection ($m = 4$):

  $$S = (\mathcal{V}' \leftarrow \mathcal{E}' \overset{1/4}{\leftarrow} \mathcal{E}' \leftarrow \mathcal{V}')^L \circ GR_4, \qquad L \geq 1.$$

  The case $L = 1$ results in linear interpolation, $L = 2$ corresponds to Loop's original scheme (for details, see [27]).

- A primal/dual family for quadrisection:

  $$S = (\mathcal{V}' \leftarrow \mathcal{F}' \overset{1/4}{\leftarrow} \mathcal{F}' \leftarrow \mathcal{V}')^L \circ GR_4,$$

  resp.

  $$S^* = (\mathcal{F}' \overset{1/4}{\leftarrow} \mathcal{F}' \leftarrow \mathcal{V}') \circ (\mathcal{V}' \leftarrow \mathcal{F}' \overset{1/4}{\leftarrow} \mathcal{F}' \leftarrow \mathcal{V}')^{L-1} \circ GR_4 \circ (\mathcal{V} \leftarrow \mathcal{F}),$$

  where $L \geq 1$. These families were independently proposed and investigated in [27] and [6].

- Kobbelt's scheme [20] for $\sqrt{3}$-subdivision:

  $$S = (\mathcal{V}' \leftarrow \mathcal{F}' \overset{1/3}{\leftarrow} \mathcal{F}' \leftarrow \mathcal{V}') \circ GR_3.$$

- The family $VFV(L)$ for $\sqrt{3}$-subdivision

$$S = (\mathcal{V}' \leftarrow \mathcal{F}' \leftarrow \mathcal{V}')^L \circ GR_3$$

and its dual counterpart

$$S = (\mathcal{F}' \leftarrow \mathcal{V}') \circ (\mathcal{V}' \leftarrow \mathcal{F}' \leftarrow \mathcal{V}')^{L-1} \circ GR_3 \circ (\mathcal{V} \leftarrow \mathcal{F})$$

$L \geq 1$, proposed in [27].

3 Smoothness Analysis and Design of Composite Schemes

3.1 Generalities on Convergence and Smoothness

The smoothness analysis of stationary subdivision schemes is usually separated into two steps, the analysis in the regular case (a mesh topology that is embedded into a 3-directional uniform mesh of $\mathbb{R}^2$) and a certain number of singular cases (in our case, this will be only the consideration of extraordinary vertices). This approach is valid only under the assumption that TR is uniform and local, and that the stencils of the GR are finite. In a more formal way, the smoothness analysis is based on viewing the limit surface (and all intermediate triangulated surfaces associated with σ^j) as covered by local charts, i.e., parametric mappings from $\mathbb{R}^2$ into $\mathbb{R}^3$, whose domains Ω_ν correspond to overlapping triangular patches F_ν in some fixed $\mathcal{T}^{j_0}$. E.g., one could consider one chart per 1-ring neighborhood of faces $N(v)$ for each $v \in \mathcal{T}^{j_0}$. Because of finite stencil support, for $j \geq j_0$ the local charts will depend only on the restriction of $(\mathcal{T}^{j_0}, \sigma^{j_0})$ to some small neighborhood $\tilde{F}_\nu$ of F_ν. Thus, by embedding these extended triangular patches $\tilde{F}_\nu \supset F_\nu$ suitably into the plane (this results in domains $\tilde{\Omega}_\nu \supset \Omega_\nu$), we can study convergence and smoothness locally by looking at the subdivision process on each $\tilde{F}_\nu$. Moreover, this can be done in a functional setting (by looking at functions from $\tilde{\Omega}_\nu \supset \Omega_\nu$ into $\mathbb{R}$ rather than into $\mathbb{R}^3$).

Simplifications come from the fact that by using the uniformity assumption on TR and choosing j_0 large enough, the patches $\tilde{F}_\nu \supset F_\nu$ and their embeddings in the plane $\tilde{\Omega}_\nu \supset \Omega_\nu$ can be chosen such that only a few different types of $\tilde{\Omega}_\nu$ occur, and that those can be viewed as part of some generic triangulations of $\mathbb{R}^2$. In other words, by using appropriate local charts as vehicle, we are able to switch from the investigation of subdivision schemes for parametric surfaces associated with arbitrary triangular mesh topologies to the investigation of subdivision schemes for scalar functions over a few special triangulations on $\mathbb{R}^2$. For triangular mesh topologies, only 2 such special triangulations are required, *a uniform type-I triangulation of* $\mathbb{R}^2$ and a *valence-k rotationally-invariant triangulation.* A type-I triangulation is shown in Fig. 6 b), and a valence-4 rotationally-invariant triangulation in Fig. 6 c), together with sample regions $\tilde{\Omega}_\nu \supset \Omega_\nu$ as they would look for Loop's scheme. Fig. 6 a) shows a planar version of the original $\mathcal{T}^{j_0}$ with $j_0 = 2$, it is easy to see that any $\mathcal{T}^2$ can be covered by families of sets

$F_\nu \subset \tilde{F}_\nu$ with enough overlap, and with regions $\tilde{\Omega}_\nu$ corresponding to either Fig. 6 b) or c).

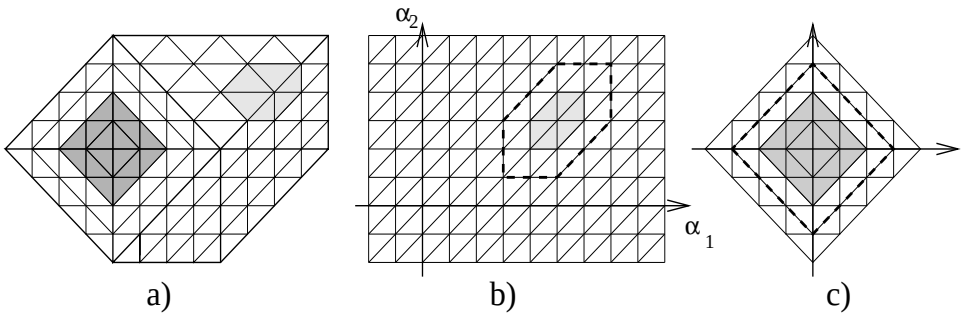


Figure 6: Examples of local patches F_μ, and their embedding into standard triangulations (F_ν and Ω_ν are shown as shaded regions, the dashed lines indicates the boundary of $\tilde{\Omega}_\nu$)

The investigation of subdivision schemes on uniform type-I triangulations is essentially complete, and more or less equivalent to the theory of *refinable vectors*. Reviews with emphasis on subdivision applications can be found in [2, 15, 19, 8, 4]. The ingredients we need to apply this theory are as follows:

- The *dimension of the refinable vector* is $r = 1$ for vertex-based, $r = 2$ for face-based, and $r = 3$ for edge-based schemes. The components of the vectors are associated with the 2 types of faces resp. 3 types of edges in a type-I triangulation.

- The *dilation matrix* M is an integer 2×2 matrix M with $\det(M) = m$ and isotropic spectrum ($|\lambda_1| = |\lambda_2| = \sqrt{m}$) which is determined by the associated TR. There are usually several possible M, and one has to fix one by assuring that M maps $\mathbb{Z}^2 = \mathcal{V}'$ onto the set $\mathcal{V}$ of old vertices $v \in \mathcal{V}$. The identification of $\mathbb{Z}^2$ with $\mathcal{V}'$ is in agreement with Fig. 7 b), and induces (through the application of M) an identification of $\mathcal{V}$ with $\mathbb{Z}^2$. E.g., with the plots in Fig. 3 properly transformed to a square lattice as shown in Fig 7 b), we get

$$M_3 = \begin{pmatrix} 2 & -1 \\ 1 & 1 \end{pmatrix}, \quad M_4 = \begin{pmatrix} 2 & 0 \\ 0 & 2 \end{pmatrix}, \quad M_7 = \begin{pmatrix} 3 & -1 \\ 1 & 2 \end{pmatrix}, \quad M_9 = \begin{pmatrix} 3 & 0 \\ 0 & 3 \end{pmatrix},$$

  for $\sqrt{3}-$, $2-$, $\sqrt{7}-$, and $3-$refinement. The identification of $\mathcal{V}$, $\mathcal{V}'$ allows us from now on to replace functions such as $\sigma_\mathcal{V}$ by $\mathbb{Z}_2$ sequences, similarly, $\sigma_\mathcal{F}$ and $\sigma_\mathcal{E}$ can be represented by $\mathbb{Z}_2$ sequences of vectors with r components.

- The *mask* $P := \{P_\alpha,\ \alpha \in \mathbb{Z}^2\}$ is a finitely supported sequence of $r \times r$ matrices describing the stencil information for S. Their definition from S is simple: In the vertex-based case, the P_α are scalars and found as the values on $\mathbb{Z}^2$ after one subdivision step if the sequence $\sigma_\mathcal{V}$ is set to 1 at the origin, and 0 at all other $0 \neq \alpha \in \mathbb{Z}^2$, i.e., if $\sigma_\mathcal{V} = \delta_0$. Since $\mathcal{V}$ is $M\mathbb{Z}^2$-shift-invariant by definition of S the

result of S applied to $\sigma_{\mathcal{V}} = \delta_\beta$ would be the same sequence but shifted by $-M\beta$. Thus, we easily obtain

$$\sigma_{\mathcal{V}'}(\alpha) = \sum_{\beta \in \mathbf{Z}^2} P_{\alpha - M\beta} \sigma_{\mathcal{V}}(\beta). \tag{4}$$

An analogous formula holds for the face- and edge-based case, with the only difference that (4) has to be understood in vector-matrix notation. In summary, in the regular case, subdivision schemes can be studied as iterations of convolution (or Toeplitz) type operators acting on vector $\mathbb{Z}^2$ sequences.

- To understand the convergence and smoothness properties of the scheme, it is convenient to study the solutions $\Phi : \mathbb{R}^2 \to \mathbb{R}^r$ associated *refinement equation*,

$$\Phi = \sum_{\alpha \in \mathbf{Z}^2} P_\alpha \Phi(M \cdot - \alpha). \tag{5}$$

and the *cascade iteration*

$$\Phi^{j+1} = \sum_{\alpha \in \mathbf{Z}^2} P_\alpha \Phi^j(M \cdot - \alpha), \qquad j \geq 0, \tag{6}$$

where $\Phi^0 : \mathbb{R}^2 \to \mathbb{R}^r$ is a compactly supported vector function. It is easy to see that if the cascade iteration produces a L_p convergent sequence Φ^j then its limit is a compactly supported L_p solution to (5).

The connection to subdivision is straightforward: If Φ^0 is chosen appropriately, then

$$g^j := \sum_{\alpha \in \mathbf{Z}^2} \sigma^j(\alpha)^T \Phi^0(M^j \cdot - \alpha) = \sum_{\alpha \in \mathbf{Z}^2} \sigma^0(\alpha)^T \Phi^j(\cdot - \alpha), \qquad j \geq 0,$$

is related to the discrete surface given by σ^j. E.g., if we look at vertex-based schemes and take as Φ^0 the piecewise linear hat function positioned at the origin of a type-I triangulation (identified with $\mathcal{T}^0$ resp. $\mathbb{Z}^2$), then g^j coincides with the piecewise linear function associated with $(\mathcal{T}^j, \sigma^j)$. Thus, convergence of the cascade algorithm implies convergence of the subdivision scheme, and the limit $g = \lim_{j \to \infty} g^j$ is represented by a linear combination of the shifts $\Phi(\cdot - \alpha)$, and thus inherits its smoothness properties from Φ. With the proper choice of Φ^0, similar interpretations hold for face- and edge-based subdivision schemes.

- As was mentioned before, the investigation of (5) resp. (6) is essentially complete. There are some issues, such as the existence of a compactly supported distributional solution Φ of (5), the *order of polynomial reproduction* (or *sum rule order*) and local linear independence of the set of shifts $\{\Phi(\cdot - \alpha) : \alpha \in \mathbb{Z}^2\}$, which can be formulated in terms of the mask P resp. its symbol

$$P(\omega) = m^{-1} \sum_{\alpha \in \mathbf{Z}^2} P_\alpha e^{-i\alpha\omega}, \quad \omega \in \mathbb{T}^2, \tag{7}$$

alone.

Convergence of the cascade iteration resp. smoothness of Φ as well as L_p-stability of the shifts $\{\Phi(\cdot - \alpha) : \alpha \in \mathbb{Z}^2\}$ need more elaborate tools. There are two basic approaches, one is via Fourier transform techniques and uses a so-called *transition operator* [15, 18, 16]

$$(T_P X)(\omega) = \sum_{\tilde{\gamma} \in \tilde{\Gamma}} P(\omega_{\tilde{\gamma}}) X(\omega_{\tilde{\gamma}}) P(\omega_{\tilde{\gamma}})^*|_{\omega_{\tilde{\gamma}} = M^{-T}(\omega + 2\pi\tilde{\gamma})}, \quad \omega \in \mathbb{T}^2, \tag{8}$$

acting on non-negative definite Hermitian $r \times r$ matrix functions $X(\omega)$ but yields a complete theory only for L_2. The set $\tilde{\Gamma}$ is a fixed representer set for $\mathbb{Z}^2/(M^T\mathbb{Z}^2)$, and consists of m elements $\tilde{\gamma}$. The second approach uses the *joint spectral radius* of the m operators

$$(A_\gamma \sigma)(\alpha) = \sum_{\beta \in \mathbf{Z}^2} P_{\gamma + M\alpha - \beta} \sigma(\beta) \tag{9}$$

with respect to a certain finite-dimensional subspace V_P determined by the mask P and its sum rule order. Here γ is chosen from a fixed representer set Γ of $\mathbb{Z}^2/(M\mathbb{Z}^2)$,

The latter approach is suitable for all L_p, $1 \le p \le \infty$, in particular, it covers the case of uniform convergence and Hölder smoothness ($p = \infty$). Its only drawback is that the practical evaluation of joint spectral radii is computationally expensive, especially if m, r, or the mask support become larger while the assessment of L_2 smoothness properties via matrix transfer operators is less involved (it leads to a matrix eigenvalue problem whose dimension is linear in the number of non-zero mask coefficients P_α, and quadratic in r). Some software tools that support these tasks are described in [19, 8]. There is one partial case where the Hölder smoothness analysis is simplified: If $r = 1$ and the scalar symbol is non-negative, i.e., $P(\omega) \ge 0$, $\omega \in \mathbb{T}^2$, then the Hölder smoothness of Φ is determined by the spectral radius of one operator $A_0|_{V_P}$, and inexpensive to find.

After a scheme has been studied for type-I triangulations, it still needs to pass the test in the remaining irregular situations which in the case of triangulations is the behavior near *extraordinary vertices* represented by k-vertex rotationally invariant triangulations with $k \neq 6$. This theory has been developed mainly in [29, 26, 31, 35, 34], and requires the study of the characteristic map which goes beyond a simple eigenvalue analysis of the local subdivision operator associated with an appropriate invariant neighborhood of the origin in the k-vertex triangulation. The rotational symmetry of the latter is explored when representing the local subdivision operator, i.e., the restriction of S to $\tilde{\Omega}_\nu$, in a discrete Fourier basis. To the best of our knowledge, this analysis is still subject to a case-by-case approach, i.e., it has not been turned into a straightforward numerical procedure (see [34] for more information). As a compromise, often only a partial analysis is performed by verifying a necessary condition [29, 26, 35] for C^1 smoothness at the extraordinary vertex, namely, the existence of a pair of subdominant eigenvalues $\lambda_2 = \lambda_3^*$ ($\lambda_1 = 1 > |\lambda_2| = |\lambda_3| > |\lambda|_\mu$, $\mu \ge 4$) associated with specific eigenvectors in the

discrete Fourier basis of the local subdivision operator, and check the soundness of the characteristic map visually. This approach seems to be acceptable in a design cycle, where one first wants to *find* a suitable method out of a variety of choices, but needs to be complemented by a more thorough analysis after a specific method has been selected. The same remark applies to checking C^α smoothness with $\alpha > 1$ at extraordinary vertices, which is a difficult subject.

3.2 Simplifications for Composite Rules

Let us return to the class (3) of composite triangular subdivision operators. By rearranging the averaging rules, we will cast it in its canonical form as vertex-based scheme:

$$S_{\mathcal{V}} = A'_N \circ \ldots \circ A'_1 \circ GR_m, \qquad A'_n = \begin{cases} AR'_n, & n = 1, \ldots, N_1, \\ (AR_{n-N_1})', & n = N_1+1, \ldots, N = N_1 + N_2. \end{cases} \tag{10}$$

Here, $(AR_n)'$ denotes the averaging rule AR_n applied on $\mathcal{T}'$. It is crucial in the rearrangement step to maintain the order in which the averaging rules AR'_n and $(AR_n)'$. In particular, this guarantees that all compositions $A'_{n+1} \circ A'_n$ make sense. It turns out (see [27] and below) that under mild conditions many properties of the original S in (3) can be deduced from properties of its associated $S_{\mathcal{V}}$, and that the investigation of the latter is simpler in many respects.

We start with the regular case, i.e., we consider the subdivision operator (10) on a uniform type-I triangulation, and study the associated refinement equation (5).

A. Due to the transformation from S to $S_{\mathcal{V}}$, the refinement equation will always be *scalar*. Having $r = 1$ will simplify the analysis.

B. The symbol (7) will come in *factorized form*. Indeed, according to the definition of the mask coefficients P_α from the subdivision rule, it is obvious that the mask $P_{\mathcal{V}}$ of $S_{\mathcal{V}}$ is obtained by convoluting the masks P_n, $n = 1, \ldots, N$ (and multiplying the result by the factor m coming from GR_M). Note that the coefficients $(P_n)_\alpha$, $\alpha \in \mathbb{Z}^2$, of P_n can be found from the result of applying the averaging rule A'_n to the corresponding δ_0-sequence, and that

$$P_n(\omega) := \sum_{\alpha \in \mathbf{Z}^2} P_{n,\alpha} e^{-j\alpha\omega}$$

(there is no scaling by m^{-1} since this is the symbol for an averaging operator on the same mesh topology, and not of a subdivision operator). As a result,

$$P_{\mathcal{V}}(\omega) = P_N(\omega) \ldots P_1(\omega), \tag{11}$$

since the factor m from GR_m is cancelled by the normalization factor m^{-1} in the definition (7) applied to $P_{\mathcal{V}}(\omega)$. Due to the normalization condition for averaging rules, we always have $P_{\mathcal{V}}(0) = 1$. Note that though $P_{\mathcal{V}}(\omega)$ is scalar, among the $P_n(\omega)$ might be $r \times r'$ matrix symbols, with $r, r' = 1, 2, 3$ corresponding to the type

of geometric entities involved in the definition of A'_n. For writing these symbols down, we identify vertices of the type-I triangulation with $\mathbb{Z}^2$ lattice points ($v_\alpha \equiv \alpha$), denote by e^1_α, e^2_α, e^3_α, the edges connecting α with $\alpha+(1,0)$, $\alpha+(0,1)$, $\alpha+(1,1)$, respectively, while f^1_α is the triangle with vertices α, $\alpha+(1,0)$, $\alpha+(1,1)$ and f^2_α the triangle with vertices α, $\alpha+(0,1)$, $\alpha+(1,1)$. Fig. 7 a) illustrates these conventions (for $\alpha = 0$, the subscript α is not shown). Then we can write down the symbols for the rules in Fig. 5. E.g., the 2×1 matrix symbol for $\mathcal{F} \leftarrow \mathcal{V}$ rules is

$$P_{\mathcal{F}\leftarrow\mathcal{V}}(\omega) = \begin{pmatrix} \frac{1}{3}(1 + e^{i\omega_1} + e^{i(\omega_1+\omega_2)}) \\ \frac{1}{3}(1 + e^{i\omega_2} + e^{i(\omega_1+\omega_2)}) \end{pmatrix},$$

the 2×2 matrix symbol for $\mathcal{F} \overset{c}{\leftarrow} \mathcal{F}$ is

$$P_{\mathcal{F}\overset{c}{\leftarrow}\mathcal{F}}(\omega) = \begin{pmatrix} 1-3c & c(1 + e^{-i\omega_1} + e^{i\omega_2}) \\ c(1 + e^{i\omega_1} + e^{-i\omega_2}) & 1-3c \end{pmatrix},$$

and 1×2 matrix symbol for $\mathcal{V} \leftarrow \mathcal{F}$ is

$$P_{\mathcal{V}\leftarrow\mathcal{F}}(\omega) = \frac{1}{6}\begin{pmatrix} 1 + e^{-i\omega_1} + e^{-i(\omega_1+\omega_2)} & 1 + e^{-i\omega_2} + e^{-i(\omega_1+\omega_2)} \end{pmatrix},$$

respectively. The mask coefficients can be read from Fig. 7 b)-d) where the action of the corresponding averaging rules on δ_0-sequences is displayed.

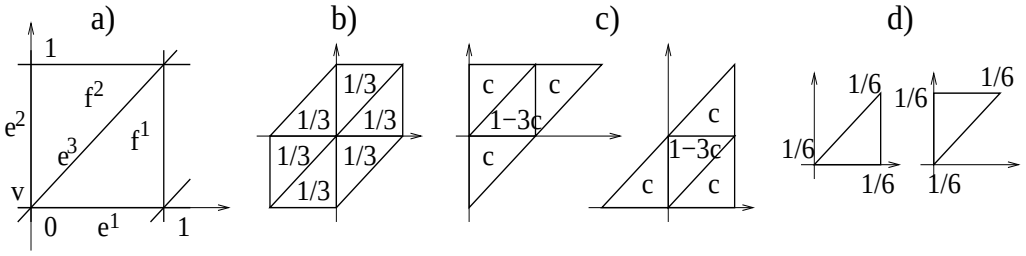


Figure 7: a) Notation for defining symbol entries ($\alpha = 0$), and results of applying b) $\mathcal{F} \leftarrow \mathcal{V}$, c) $\mathcal{F} \overset{c}{\leftarrow} \mathcal{F}$, resp. d) $\mathcal{V} \leftarrow \mathcal{F}$ to the corresponding δ_0-sequences

C. The factorization can be used to verify *sum rule orders* which are related to the order of polynomial reproduction of the subdivision scheme. Loosely speaking, $S_\mathcal{V}$ has sum rule order $K \geq 1$ if it preserves polynomial sequences of degree $\leq K-1$ (at least, for the situation of uniform type-I triangulations). In particular, $S_\mathcal{V}$ has sum rule order 1 if it preserves constants, i.e., if $S_\mathcal{V}\{1\} = \{1\}$, which is easy to verify directly. Among the many equivalent definitions of sum rule orders, we mention the following algebraic condition in terms of the symbol: $S_\mathcal{V}$ has sum rule order K if $P_\mathcal{V}(0) = 1$ (this is always satisfied) and

$$\frac{\partial^\mu P_\mathcal{V}}{\partial \omega^\mu}(2\pi M^{-T}\tilde{\gamma}) = 0 \qquad \forall\, |\mu| < K \quad \forall\, 0 \neq \tilde{\gamma} \in \tilde{\Gamma}. \tag{12}$$

Without loss of generality, we have assumed that 0 is one of the representers from $\tilde{\Gamma}$.

Given two composite rules $S_{\mathcal{V}}^{(1)}$ and $S_{\mathcal{V}}^{(2)}$ for the same TR, we define their *concatenation* $(S^{(2)}S^{(1)})_{\mathcal{V}}$ as the composite scheme, where after GR_m first the averaging rules for $S_{\mathcal{V}}^{(1)}$ and then the averaging rules for $S_{\mathcal{V}}^{(2)}$ are performed in their respective orders.

Lemma 1 *If $S_{\mathcal{V}}^{(1)}$, $S_{\mathcal{V}}^{(2)}$ are two subdivision operators given by (10), with sum rule orders K_1, K_2 (w.r.t. the same M), then their concatenations $(S^{(2)}S^{(1)})_{\mathcal{V}}$ and $(S^{(1)}S^{(2)})_{\mathcal{V}}$ coincide, and have at least sum rule order $K_1 + K_2$.*

The elementary proof directly follows from the algebraic definition (12) using the Leibnitz rule for partial differentiation of the product $P^{(2)})_{\mathcal{V}}(\omega)P^{(1)})_{\mathcal{V}}(\omega) = P_{\mathcal{V}}^{(1)}(\omega)P_{\mathcal{V}}^{(2)}(\omega)$ which represents the symbol of the composite operators (scalar multiplication is commutative). The lemma can also be applied to find the sum rule order of a given $S_{\mathcal{V}}$ if the defining sequence of AR contains intermediate mappings to vertex-based information. A special corollary is as follows: *If the scheme $S_{\mathcal{V}}$ defined in (10) has sum rule order K, then $S_{\mathcal{V}}^L$ (the L-fold concatenation of $S_{\mathcal{V}}$) has sum rule order LK*. This allows us to obtain subdivision schemes with higher sum rule orders from schemes with $K = 1$ or $K = 2$ without difficulty, as was the case in some of the examples at the end of Section 2. Higher-order sum rule orders are prerequisite for achieving schemes with very smooth limit surfaces.

D. Since $r = 1$ and factorizations hold, simplifications in the *smoothness analysis* are possible. First of all, the formula for the transition operator simplifies to

$$(T_{P_{\mathcal{V}}}X)(\omega) = \sum_{\tilde{\gamma}\in\tilde{\Gamma}} |P_{\mathcal{V}}(\omega_{\tilde{\gamma}})|^2 X(\omega_{\tilde{\gamma}}), \qquad \omega_{\tilde{\gamma}} = M^{-T}(\omega + 2\pi\tilde{\gamma}), \quad \omega \in \mathbb{T}^2, \tag{13}$$

and solely depends on the squared symbol $|P_{\mathcal{V}}(\omega)|^2 \geq 0$, and the L_2-smoothness issue is completely covered in [9, 17], where also references to previous work can be found. Software for computing the best possible values of the Sobolev smoothness exponent of the associated refinable function $\Phi_{\mathcal{V}}$ based on these papers (and the later [18, 16] for the vector case) is available from the webpages of the authors of [19], [7, 8], [30].

Let us be a bit more concrete on the estimation of *Hölder smoothness exponents* of $\Phi = (\Phi_1, \ldots, \Phi_r)^T$:

$$s_\infty(\Phi) = \inf\{s \geq 0 : \ \Phi_l \in C^s(\mathbb{R}^2), \ l = 1, \ldots, r\}.$$

There are 3 basic approaches. The trivial lower bound

$$s_\infty(\Phi) \geq s_2(\Phi) - 1$$

follows from the embedding $H^{s+1+\epsilon}(\mathbb{R}^2) \subset C^s(\mathbb{R}^2)$, $s \geq 0$, $\epsilon > 0$, and relates the Hölder exponent to the L_2-Sobolev exponent $s_2(\Phi)$ which is easier to obtain ([8, 11] promote this approach).

Secondly, for concatenated schemes one can use convolution arguments: If the refinable functions $\Phi_{\mathcal{V}}^{(i)}$ corresponding to the subdivision operators $S_{\mathcal{V}}^{(i)}$ have Hölder exponents $s_\infty(\Phi_{\mathcal{V}}^{(i)}) > 0$, $i = 1, 2$, then the refinable function associated with the concatenated scheme $(S^{(1)}S^{(2)})_{\mathcal{V}} = (S^{(2)}S^{(1)})_{\mathcal{V}}$ is given by convolution $\Phi = \Phi_{\mathcal{V}}^{(1)} * \Phi_{\mathcal{V}}^{(2)}$, and thus satisfies

$$s_\infty(\Phi) \geq s_\infty(\Phi_{\mathcal{V}}^{(1)}) + s_\infty(\Phi_{\mathcal{V}}^{(2)}).$$

Although this inequality is not necessarily sharp, it allows us to reduce the consideration for complicated concatenated schemes to estimates for Hölder smoothness exponents of their components which might be easier to obtain. In particular, for the refinable function $\Phi_{\mathcal{V}}^L$ associated with the L-fold concatenation $S_{\mathcal{V}}^L$ of $S_{\mathcal{V}}$, this approach gives the lower bound $s_\infty(\Phi_{\mathcal{V}}^L) \geq L s_\infty(\Phi_{\mathcal{V}})$, i.e., guarantees linear growth of the Hölder smoothness for $L \to \infty$, if $s_\infty(\Phi_{\mathcal{V}}) > 0$. This fact has been explored in [6].

Finally, we can use the joint spectral radius criterion [9, 16] which gives the precise geometric decay of the K-th order differences of the subdivision sequences σ^j (that estimating this decay is crucial for proving Hölder continuity of limit surfaces in subdivision processes is well-known, and has been used in many papers, see [2, 4]). Since computable lower and upper bounds for the joint spectral radius converge very slowly to the exact value while requiring large computational resources, it is very desirable to use shortcuts whenever possible. We mention one partial case of composite schemes where the Hölder exponent can be computed in an efficient way: If L is *even* and the symbol $P_{\mathcal{V}}(\omega)$ of a composite scheme $S_{\mathcal{V}}$ is real-valued, then the concatenated scheme $S_{\mathcal{V}}^L$ has obviously a non-negative symbol $P_{\mathcal{V}}(\omega)^L \geq 0$. Consequently, $s_\infty(\Phi_{\mathcal{V}}^L)$ is computable as the spectral radius of a single matrix, see e.g. [14].

E. What concerns the quality of composite triangular subdivision schemes near extraordinary vertices with valence $k \neq 6$, some interesting observations have been made in [27]. It turns out that normally the C^1 property holds for all valences, with the exception of $k = 3$. To overcome the problems for $k = 3$, and to obtain visually pleasing surfaces after a few subdivision steps, some modifications of the basic AR have been proposed in [27]. E.g., if the basic rule $\mathcal{F} \leftarrow \mathcal{V}$ is among the averaging rules then it can be modified as shown in Fig. 8 a), where a special weight factor $w = w(k)$ is introduced if one of the vertices of the triangle has valence $k \neq 6$. Note that triangles with more than one extraordinary vertex can appear only in the first subdivision step. It has been observed that often a slight increase $w > 0$ is sufficient for proving the C^1 property at vertices of valence $k = 3$, and that choices $w(k) > 0$ for $k < 6$ and $w(k) < 0$ for $k > 6$ improve the fairness

of the discrete surfaces. Almost any of the basic AR in Figure 5 could potentially be modified near extraordinary vertices. Fig. 8 b) and c) show such modifications for $\mathcal{F} \stackrel{c}{\leftarrow} \mathcal{F}$ resp. for $\mathcal{V} \leftarrow \mathcal{F}$ (in [27], the latter was called flap modification).

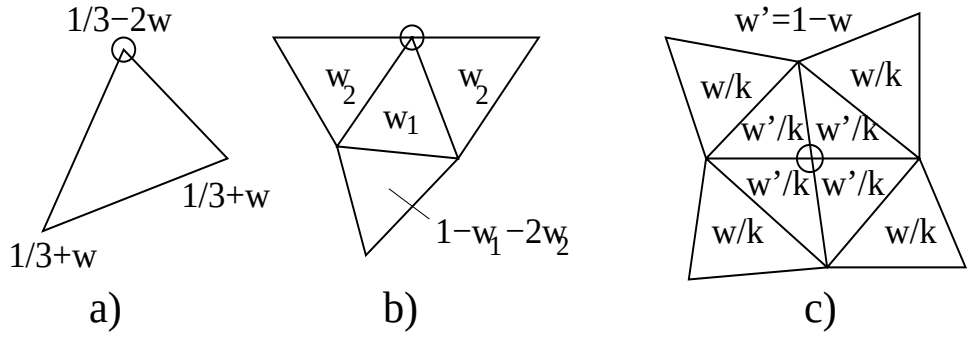


Figure 8: Weight modifications for a) $\mathcal{F} \leftarrow \mathcal{V}$, b) $\mathcal{F} \stackrel{c}{\leftarrow} \mathcal{F}$, and c) $\mathcal{V} \leftarrow \mathcal{F}$

Unfortunately, in contrast to the regular case, there are currently no simplifying statements that apply to the smoothness analysis of composite schemes near extraordinary vertices. E.g., concatenation of "good" rules may not necessarily result in a good scheme (at least, there is no proof for such a result, and visual examination for the critical valence $k = 3$ does not suggest anything). The only general result for composite schemes, which holds both in the regular and irregular cases, is about the connection of the smoothness properties of the general composite subdivision operator S given by (3) and its vertex-based rearrangement $S_{\mathcal{V}}$ given by (10). It turns out that under mild assumptions on (3) the properties of S cannot be worse than those of $S_{\mathcal{V}}$. More precisely, we have the following

Lemma 2 *Let S and $S_{\mathcal{V}}$ be defined by (3) and (10), respectively, and assume that the part*

$$S' := AR'_{N_2} \circ \ldots \circ AR'_1 \circ GR_m$$

of S preserves constant sequences. Then the subdivision scheme S converges for generic bounded initial data to a $C^{\alpha}_{\mathrm{loc}}$ limit surface if $S_{\mathcal{V}}$ does so. More precisely, if ϕ_v is the limit of recursively applying $S_{\mathcal{V}}$ to the delta-sequence δ_v associated with a vertex $v \in \mathcal{V}^0$ then the limit ϕ_x under the recursive application of S to a delta-sequence δ_x associated with a geometric entity x from X^0 can be represented as a linear combination of the former (the coefficients of which are determined by the composite averaging rule $AR_{N_1} \circ \ldots \circ AR_1$).

The proof of this result is essentially the same as the one given in [27] for the particular case $AR_1 = \mathcal{V} \leftarrow \mathcal{F}$ ($N_1 = 1$), and will not be reproduced here.

3.3 Design Rules

From the above, we summarize the following design approach to subdivision schemes covering both the triangular and, via duality, hexagonal mesh case.

A Determine the type of topological refinement, and dilation factor m. On a regular type-I triangulation, fix the corresponding dilation matrix M.

B By using the trivial subdivision operator GR_m and a few basic averaging rules $A_i = X_i \leftarrow X_{i-1}$, where $i = 1, \ldots, N$ and $X_0 = X_N = \mathcal{V}$, compose a vertex-based subdivision operator $S_{\mathcal{V}}$ as in (10) such that it reproduces at least constant sequences, preferably, linear sequence functions, i.e., possesses sum rule order $K = 1$ or $K = 2$. The verification for $K = 2$ may be confined to the situation of a regular type-I triangulation. If the interest is in primal hexagonal schemes (or dual triangular schemes), make sure that among the X_i with $i = 1, \ldots, N-1$ there is at least one $\mathcal{F}$. This whole task depends on the topological refinement rule, and requires some qualified guesses. However, it is usually not difficult to come up with one or several such lower-order composite rules by using as few as possible AR_i.

C Suppose that such a candidate $S_{\mathcal{V}}$ has been found. Then consider the family $S_{\mathcal{V}}^L$, $L \geq 1$, and check its properties in the regular case using the theory of refinable functions. For $L \leq 4$ this can usually be done with the software tools developed in [19, 7, 11], while for large L good lower smoothness estimates follow from the outlined convolution argument. It is also recommended to investigate the stability of the set of shifts $\{\Phi(\cdot - \alpha),\ \alpha \in \mathbb{Z}^2\}$ and the Sobolev regularity, as this might be of interest for applications of the subdivision approach in simulations. If m or the complexity of $S_{\mathcal{V}}$ are increasing, the exact computation of Hölder exponents might become impractical, and one might restrict the attention to $L = 2, 4$, where $P_{\mathcal{V}}(\omega)^L \geq 0$. Finally, if several candidate $S_{\mathcal{V}}$ are available then other suitable concatenations besides $S_{\mathcal{V}}^L$ may be tried.

D Among the cases investigated in the last step, choose a scheme which has Hölder smoothness $s_\infty >> 2$, i.e., is safely C^2 on regular grids, and investigate the associated local subdivision operator for a $k(\neq 6)$-vertex rotationally invariant triangulation. This investigation involves some modification of one or several of the A_i near the extraordinary vertex, as suggested in the previous subsection. To achieve the C^1-property globally, such modifications are necessary only for low-valence cases such as $k = 3$ but may later be useful for further fairing as well.

E Under the assumptions of Lemma 2, the results of the analysis of $S_{\mathcal{V}}$ automatically hold for those vertex- (primal), face- (dual), and edge-based composite schemes S of the form (3) which are given by proper rearrangements of the components of $S_{\mathcal{V}}$ as discussed above. In particular, if S with $X_0 = Y_{N_2} = \mathcal{F}$ are among the admissible rearrangements of $S_{\mathcal{V}}$, then we arrive at hexagonal schemes. This makes a separate analysis for the hexagonal case unnecessary.

F Finally, the analysis needs to be complemented by the modification of the rules near the boundary of a triangulation. This is not a trivial task for larger m, unless m is of the form $m = 2^p 3^q$, where it has been essentially solved, see [23, 20, 3] for $m = 3, 4$. Clearly, achieving a sufficient degree of local smoothness analysis is one thing, fair surfaces sometimes a quite different one.

4 Hex-by-7 Subdivision Schemes

In this concluding section, we will follow the above design approach for hex-by-7 subdivision. It seems that until now there is no general proposal for this type of hexagonal refinement, which makes this a non-trivial test case. Note that the more popular cases $m = 3$ ($\sqrt{3}$-subdivision [20, 27, 19, 3]) and $m = 4$ (quadrisection) have been discussed from the point of view of composite schemes in [27], and that $m = 7$ is the next admissible dilation factor for triangular meshes. The motivation for hex-by-7 is not so much a matter of the theory of subdivision surfaces or an anticipated need for another algorithm for surface modelling but the potential use in other applications, e.g., pyramid algorithms for human vision modeling or terrain description in geophysics, where hexagonal grids have been popular for various reasons. The hex-by-7 refinement offers some directional features which can be built into wavelet spaces associated with the multiscale ladders of subspaces defined by the subdivision operator.

A: First of all, we have $m = 7$, and choose

$$M = \begin{pmatrix} 2 & 1 \\ -1 & 3 \end{pmatrix} \tag{14}$$

to describe the dilation on a uniform type-I triangulation. On a uniform hexagonal grid, this corresponds to a counter-clockwise grid rotation by $\phi = \arctan(\sqrt{3}/5)$, whereas the alternative choice

$$M = \begin{pmatrix} 3 & -1 \\ 1 & 2 \end{pmatrix} \tag{15}$$

corresponds to a clockwise rotation by the same angle, this latter case was shown in Figure 3 c). In order to apply our analysis tools as is, the rotation pattern (i.e., M) has to be the same in all subdivision steps. On general triangulations, this consistency in choosing the refinement pattern corresponds to assuming an *orientable triangulation*. More precisely, we assume that any face $f \in \mathcal{F}$ is given by an *ordered* vertex triple $f = (v_1, v_2, v_3)$ or

$$f \; : \quad v_1 \to v_2 \to v_3 \to v_1$$

which is consistent on the set of all faces: If $e = (v, v') = f \cap f'$ is the common edge of two triangles then its endpoints satisfy $v \to v'$ in exactly one of the ordered vertex representations corresponding to f and f'. Obviously, there are triangulations (such as an trianglated Möbius band) which cannot be oriented in the above sense. If the triangulation is orientable, then the $\sqrt{7}$-refinement consistent with the dilation M from (14) consists of inserting 3 new vertices per old triangle f as in Fig. 9 a). Note that the

orientation induces a unique association $v_i' \leftrightarrow (f, v_i, e_i)$ between new vertices and old triangles, vertices, and edges. To see the uniformity of this TR, the location of v_i' is given by barycentric coordinates of $(4/7, 2/7, 1/7)$ with respect to f and the vertex ordering (v_i, v_{i+1}, v_{i+2}), $i = 1, 2, 3$ (here, $v_4 = v_1$, $v_5 = v_2$). A portion of the refined triangulation $\mathcal{T}' = (\mathcal{V}', \mathcal{F}')$ is depicted in Fig. 9 b), it inherits its orientation from $\mathcal{T} = (\mathcal{V}, \mathcal{F})$. It is important to realize that on general triangulations, the two possible orientations lead to different mesh connectivity (and thus different $\mathcal{T}$) in the way the newly inserted vertices are connected accross old edges: We always have a new edge between two vertices associated with the same old edge (the other new edges are between a new vertex and its associated old vertex, and between new vertices if they are associated with the same old vertex and neighboring f).

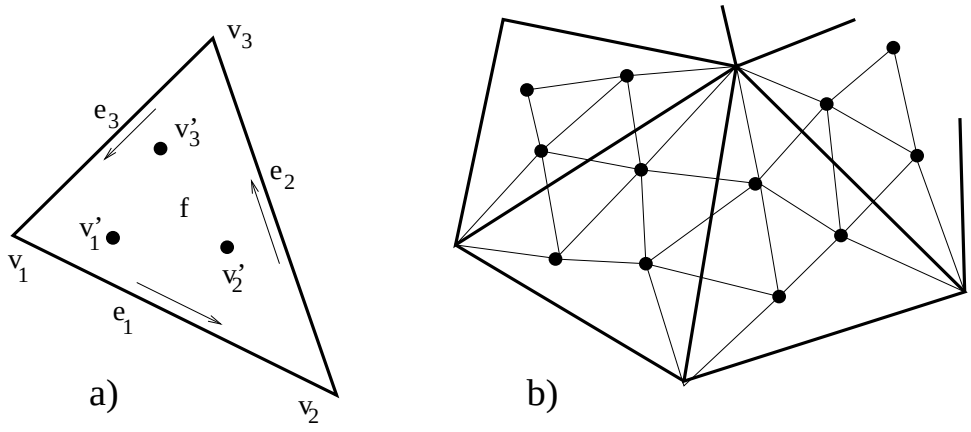


Figure 9: Vertex insertion and $\sqrt{7}$-refinement associated with M given by (14)

Note that in some papers an alternation of the orientation between two consecutive refinement steps has been proposed. This corresponds to alternating the two dilation matrices in (14) and (15), and could still be analyzed by realizing that two consecutive alternating $\sqrt{7}$-refinements are essentially equivalent to a 7-refinement (the same trick was initially applied for $\sqrt{3}$-refinement [1]). However, this leads to $m = 49$ for the new subdivision scheme comprising two alternating $\sqrt{7}$-subdivision steps, with the consequence that the smoothness analysis would require extensive computational efforts.

B: The next step is the invention of some lower-order composite vertex-based schemes with a subdivision operator $S_{\mathcal{V}}$ of the form (10). Clearly, following previous approaches to composite schemes with $m = 3$ and $m = 4$, one would first try to *factorize* the subdivision operator $S_{\mathcal{V}}^{lin}$ associated with the natural linear interpolatory scheme for this refinement. The latter is given by linearly interpolating the values at the old vertices $\mathcal{V}$ within each old triangle f using local barycentric coordinates, und inheriting the values at the new vertices $v' \in f$ from this local interpolant. This yields the stencil shown in Fig. 10 a) for the new vertices. Unfortunately, this elementary subdivision rule cannot be factored into the form (10), with the additional requirement that at least one of the basic averaging rules A_i' involves $\mathcal{F}'$. There exists a bit unconventional factorization for

$S_{\mathcal{V},lin}$ only involving edge- and vertex-based averaging rules:

$$S_{\mathcal{V},lin} \; : \quad (\mathcal{V}' \leftarrow \mathcal{E}' \overset{c_3}{\leftarrow} \mathcal{E}' \overset{c_2}{\leftarrow} \mathcal{E}' \overset{c_1}{\leftarrow} \mathcal{E}' \leftarrow \mathcal{V}') \circ GR_7, \tag{16}$$

where the constants c_i can be determined as the roots of a cubic polynomial (but are not rational). Since we are mainly interested in families containing dual schemes as well, we will not elaborate further on $S_{\mathcal{V},lin}$ and its factorization (16) but rather look for alternatives.

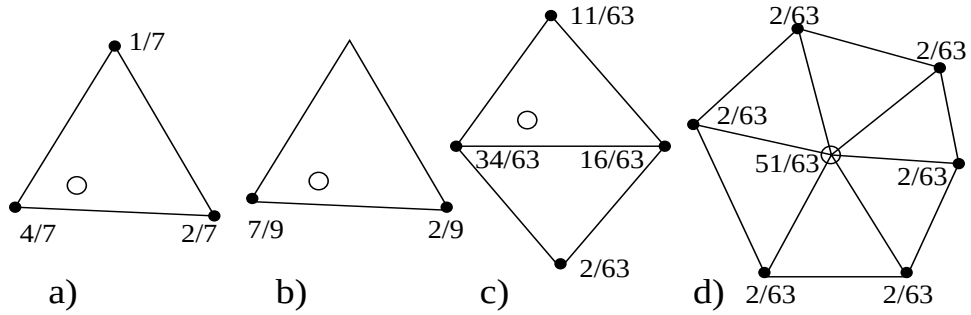


Figure 10: Stencils for new vertex positions for the interpolatory schemes a) $S_{\mathcal{V},lin}$, b) $S_{\mathcal{V},4/7}$, and for c) new and d) old vertices for the approximating scheme $S_{\mathcal{V},4/7,6/7}$

We will look for an as compact as possible interpolatory composite scheme which involves $\mathcal{F} \leftarrow \mathcal{V}$, $\mathcal{F} \overset{c}{\leftarrow} \mathcal{F}$, and $\mathcal{V} \leftarrow \mathcal{F}$. We start with the one-parameter family

$$S_{\mathcal{V},c} \; : \quad (\mathcal{V}' \leftarrow \mathcal{F}' \overset{c}{\leftarrow} \mathcal{F}' \leftarrow \mathcal{V}') \circ GR_7, \tag{17}$$

and try to fix the parameter c such that $S_{\mathcal{V},c}$ reproduces at least constants. This is straightforward, since the result of $S_{\mathcal{V},c}$ applied to a δ-sequence centered at an arbitrary $v \in \mathcal{V}$ can easily be found. The process is depicted in Figure 11 a)-c) for a uniform type-I partition. Obviously, the scheme is interpolatory and reproduces constants iff $c = 4/7$. The stencil for new vertices associated with this scheme is more economic than the one for the linear interpolatory scheme, and depicted in Fig. 10 b). On the downside, it is easy to realize that the scheme does not reproduce linear grid sequences.

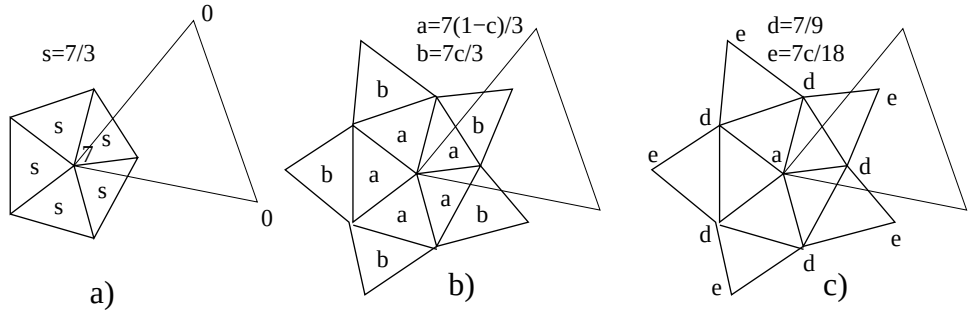


Figure 11: Derivation of $S_{\mathcal{V},c}$: a) GR_7 and $\mathcal{F}' \leftarrow \mathcal{V}'$, b) $\mathcal{F}' \overset{c}{\leftarrow} \mathcal{F}'$, and c) $\mathcal{V}' \leftarrow \mathcal{F}'$

The fact that $S^L_{\mathcal{V},4/7}$ has only sum rule order $K = 1$ has the consequence that $S^L_{\mathcal{V},4/7}$ will have sum rule order L (and not $2L$). Thus, to achieve the C^2-property in the regular case one would need at least $L \geq 3$. A simple fit for this deficiency is to extend $S_{\mathcal{V},4/7}$ by another averaging rule, e.g., of the form $\mathcal{V} \stackrel{c'}{\leftarrow} \mathcal{V}$. It is an easy exercise to find out that $c' = 6/7$ will yield reproduction of linear grid functions in the regular case, and we arrive at a second candidate scheme from the family

$$S_{\mathcal{V},c,c'} \; : \quad (\mathcal{V}' \stackrel{c'}{\leftarrow} \mathcal{V}' \leftarrow \mathcal{F}' \stackrel{c}{\leftarrow} \mathcal{F}' \leftarrow \mathcal{V}') \circ GR_7, \qquad c = 4/7,\ c' = 6/7. \tag{18}$$

This scheme is not interpolatory anymore, see Fig. 10 c) and d) for the stencils for newly inserted and old vertices in the regular case. Note that for extraordinary vertices, one could try to carefully choose the parameter $c' = c'(k)$ in the $\mathcal{V} \stackrel{c'}{\leftarrow} \mathcal{V}$ rule as a function of $k \neq 6$, to achieve the C^1 property but we will not pursue this at the moment.

There might be other attractive lower-order composite schemes which reproduce constants, and preferably also linear functions in the regular case, but we will restrict our attention to the further investigation of the above examples.

C: We come to the analysis of the L-fold concatenations $S^L_1 := S^L_{\mathcal{V},lin}$, $S^L_2 := S^L_{\mathcal{V},4/7}$, $S^L_3 = S^L_{\mathcal{V},4/7,6/7}$ of the above basic subdivision sches for values $L \leq 4$ in the regular case. For this, we need the symbols for $L = 1$ which can easily be obtained as follows:

$$P_1(\omega) = \frac{1}{7}\left(1 + \left\{\frac{4}{7}\sum_{\alpha\in\Lambda_1} + \frac{2}{7}\sum_{\alpha\in\Lambda_2} + \frac{1}{7}\sum_{\alpha\in\Lambda_3}\right\} e^{-i\alpha\omega}\right),$$

$$P_2(\omega) = \frac{1}{7}\left(1 + \left\{\frac{7}{9}\sum_{\alpha\in\Lambda_1} + \frac{2}{9}\sum_{\alpha\in\Lambda_2}\right\} e^{-i\alpha\omega}\right),$$

and

$$P_3(\omega) = \frac{1}{441}\left(54 + \left\{34\sum_{\alpha\in\Lambda_1} + 16\sum_{\alpha\in\Lambda_2} + 11\sum_{\alpha\in\Lambda_3} + 2\sum_{\alpha\in\Lambda_4}\right\} e^{-i\alpha\omega}\right),$$

where the index sets $\Lambda_i \subset \mathbb{Z}^2$ are obvious from the definition of the schemes. More precisely, Λ_1 contains the vertices in the 1-ring around the origin, $\Lambda_3 = 2\Lambda_1$ belongs to the 2-ring around the origin, the remaining vertices of this 2-ring form Λ_2, and Λ_4 is a certain subset of the 3-ring around the origin. All three symbol functions are real-valued for $\omega \in \mathbb{T}^2$, and possess the symmetries typical for regular triangular meshes (see [8, 7, 11] for how to explore those). One can check that among the above, only the symbol of the linear interpolatory scheme $P_1(\omega)$ is non-negative on the torus $\mathbb{T}^2$. Clearly, in addition $P_i(\omega)^L \geq 0$, $\omega \in \mathbb{T}^2$, for even L which can be used to speed up the computation of Hölder smoothness exponents.

In Table 1 below, we have used the methods described in [19]. We report our numerical predictions for Sobolev and Hölder smoothness exponents. In most cases, these are the exact exponents (if numbers are bold-faced we can formally prove this). In the remaining cases, we are at least sure that the integer part of s_∞ is correct. The important output of this exercise is the confirmation of observations made for similar families

	Family S_1^L			Family S_2^L			Family S_3^L		
L	KL	s_∞	s_2	KL	s_∞	s_2	KL	s_∞	s_2
1	2	**0.8708**	**1.6464**	1	0.3756	**0.8023**	2	1.3463	**1.9111**
2	4	**3.2929**	**3.8698**	2	**1.6046**	**1.9814**	4	**3.8223**	**3.9962**
3	6	**5.5638**	**5.9571**	3	2.9354	**2.9985**	6	5.9627	**5.9998**
4	8	**7.7397**	**7.9863**	4	**3.9629**	**3.9999**	8	**7.9923**	**7.9999**

Table 1: Sum rule orders, Hölder, and Sobolev smoothness exponents

$S_\mathcal{V}^L$ associated with TR with dilation factor $m = 3, 4$. E.g., when L is increased then the predictions for Sobolev and Hölder exponents quickly approach their theoretical limit KL, where $K = 1, 2$ is the sum rule order of the corresponding basic scheme. In all cases we have numerically checked that the shifts of the associated refinable functions are stable (this requires to establish the strict positivity of the eigenfunction of the transition operator (13) corresponding to the largest eigenvalue $\lambda = 1$, see [19]).

In particular, the schemes S_1^2, S_2^3, and S_3^2 already yield C^2 (or even C^3) limits for regular mesh topologies. This makes them candidates for further investigation. Another such candidate is the concatenation of $S_2 = S_{\mathcal{V},4/7}$ with $S_3 = S_{\mathcal{V},4/7,6/7}$. For this scheme, we have found

$$K = 3, \qquad 2.2637 \leq s_\infty \leq 2.8591, \qquad s_2 = \mathbf{2.9921}.$$

The estimates for the Hölder exponent have been computed by the joint spectral radius method, and we predict the upper bound to coincide with the exact value. Similarly, we could concatenate S_2 with $S_1 = S_{\mathcal{V},lin}$ yielding slightly worse values of

$$K = 3, \qquad 2.1646 \leq s_\infty \leq 2.7033, \qquad s_2 = \mathbf{2.9556}. \tag{19}$$

Because of the presence of S_2, these concatenated schemes (as well as S_2^3 and S_3^2 but not S_1^2) can easily be turned into schemes for hexagonal meshes by duality. Note that among those, the smallest mask is obtained for the last scheme (the concatenation of S_1 and S_2) which will be denoted by S and further investigated below.

D: The smoothness investigation and modifications of composite schemes near extraordinary vertices will be illustrated on the example of the scheme

$$S = (S_2 S_1) = (\mathcal{V}' \leftarrow \mathcal{F}' \overset{4/7}{\leftarrow} \mathcal{F}' \leftarrow \mathcal{V}') \circ S_{\mathcal{V},lin}. \tag{20}$$

Our goal is to guarantee at least C^1 smoothness globally. To this end, because of the separation of the extraordinary vertices during the refinement process it is sufficient to investigate the local subdivision map in a sufficently large neighborhood of the origin of a k-vertex rotationally invariant triangulation $\mathcal{T}$. Since the above S results in relatively small stencils, a 2-ring of triangles around the k-vertex will do (the reader can easily check that no vertex location outside this 2-ring can influence the limit surface in the vicinity of the k-vertex). Using the notation introduced in Fig. 12 and by carefully

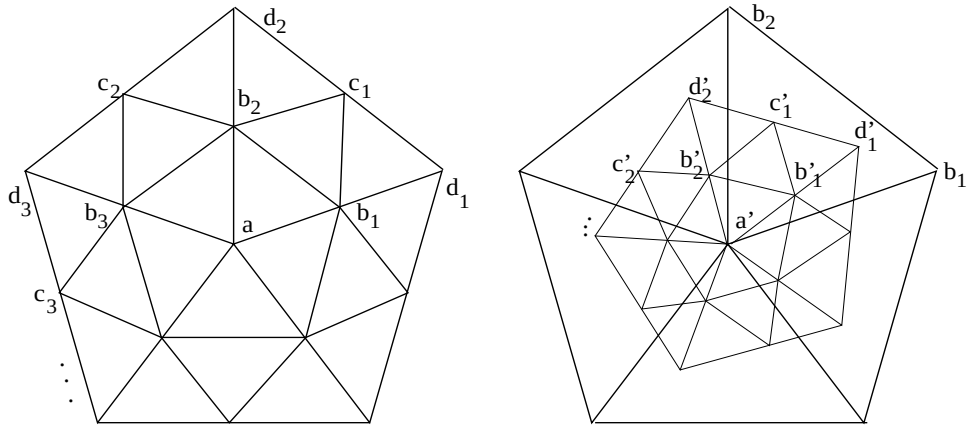


Figure 12: Notation for the local subdivision map

applying the subdivision operator S, we see that the values a', b'_i, c'_i, d'_i associated with the vertices of this 2-ring in the refined partition $\mathcal{T}'$ are given by the formulae

$$\begin{aligned}
a' &= \frac{85}{147}a + \frac{62}{147k}\sum_{j=1}^{k} b_j, \\
b'_i &= \frac{1}{882}(392a + 8b_{i-2} + 62b_{i-1} + 220b_i + 162b_{i+1} + 30b_{j+2} + 4b_{i+3} + 4c_i), \\
c'_i &= \frac{1}{882}(220a + 8b_{i-1} + 162b_i + 392b_{i+1} + 62b_{j+2} + 30c_i + 8c_{i+1} + 4d_{i+1}), \\
d'_i &= \frac{1}{882}(162a + 30b_{i-1} + 392b_i + 220b_{i+1} + 4b_{j+2} + 4c_{i-1} + 62c_i + 8d_i),
\end{aligned}$$

$i = 1, \ldots, k$ (all sequences are extended from this index set to all of $\mathbb{Z}$ by k-periodicity). To study the eigenvalues and eigenvectors of this $3k+1$-dimensional block-circulant local subdivision operator S_0, it is customary to switch within the b, c and d-blocks to the DFT basis of length k, and to reorder the whole matrix correspondingly. This leads to a block-diagonal matrix representation of S_0 with the same eigenvalues. The diagonal blocks consist of a 4×4 matrix

$$B_0 = \frac{1}{882}\begin{pmatrix} 510 & 372 & 0 & 0 \\ 392 & 486 & 4 & 0 \\ 220 & 620 & 38 & 4 \\ 162 & 646 & 66 & 8 \end{pmatrix},$$

which corresponds to the equation for a' and the 3 transformed equations associated with the DFT vector $(1, \ldots, 1)^T$, and 3×3 matrices $B_j = B(e^{i2\pi j/k})$, $j = 1, \ldots, k-1$, associated with the other $k-1$ DFT vectors of length k, where

$$B(z) = \frac{1}{882}\begin{pmatrix} 8z^{-2} + 62z^{-1} + 220 + 162z + 30z^2 + 4z^3 & 4 & 0 \\ 4z^{-1} + 162 + 392z + 62z^2 & 30 + 8z & 4z \\ 30z^{-1} + 392 + 220z + 4z^2 & 4z^{-1} + 62 & 8 \end{pmatrix},$$

is the (partial) symbol for the above block-circulant matrix. The set of eigenvalues of B_0 is $\{1,\ 1/7,\ 0.0383...,\ 0.0003...\}$ while the maximum (in absolute value) of all eigenvalues from the remaining B_j is attained in the blocks B_1 and B_{k-1}. This follows from the fact that $\rho(t) = \max|\lambda(B(e^{it})| = \max|\lambda(B(e^{-it})|$ is monotonously decreasing on $[0, \pi]$, see Fig. 13 a). It turns out that $\rho(2\pi/3) = 1/7$, and we conclude that for $k > 4$ there is a pair $\{\lambda_2, \lambda_3\}$ of subdominant eigenvalues $1 = \lambda_1 > |\lambda_2| = |\lambda_3| > |\lambda_4| \geq ...$ which are conjugate to each other and belong to B_1 resp. B_{k-1}. This is the standard situation in which the C^1 property typically holds (see [29]). For $k = 3$ this is no longer true since we have a triple $|\lambda_2| = |\lambda_3| = \lambda_4 = 1/7$ of subdominant eigenvalues, the additional one coming from the block B_0.

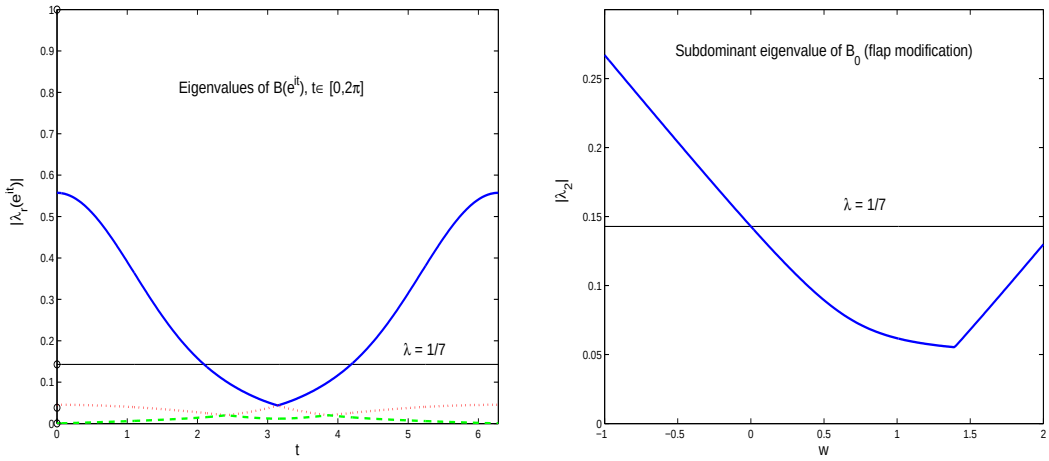


Figure 13: a) Eigenvalue distribution of B_0 and $B(e^{it})$, and b) variation of the subdominant eigenvalue of B_0 as function of the weight w if flap modification is used

Since a mathematically rigorous treatment would require the study of the characteristic map [29, 31, 35], which would become very technical and lead us away from our basic task of demonstrating the proposed design approach via composite schemes, we retreat to a visual inspection. In Figure 14, we show the result of $J = 3$ subdivision steps with the operator S applied to a (symmetric) double pyramid over a regular k-gon as initial configuration. Thus, $\mathcal{T}^0$ contains $2k$ triangular faces, two vertices of valence k, and k vertices (along the base) of valence 4. We show the cases $k = 3, 4, 5, 12$, the pictures clearly support the above findings.

Obviously, for $k = 3$ we need to fix the C^1 property but there is also some desire to generally improve the shape of the resulting surfaces for $k \neq 6$ (e.g., the surface becomes very flat near the tip of the original pyramid for $k = 12$). Within the context of composite schemes, this can most elegantly be done by modifying one or several of the AR involved. This idea was first proposed in [27]. In our example, this can be done in several ways, see the rules in Fig. 8. The easiest to analyze (and by chance also the one leading to the best visual effects) is the flap modification from Fig. 8 c). Indeed, if for valence $k \neq 6$ the modified $\mathcal{V} \leftarrow \mathcal{F}$ rule with $w \neq 0$ is applied then this modifies only the value a' at the origin of the k-vertex rotationally invariant neighborhood (all other

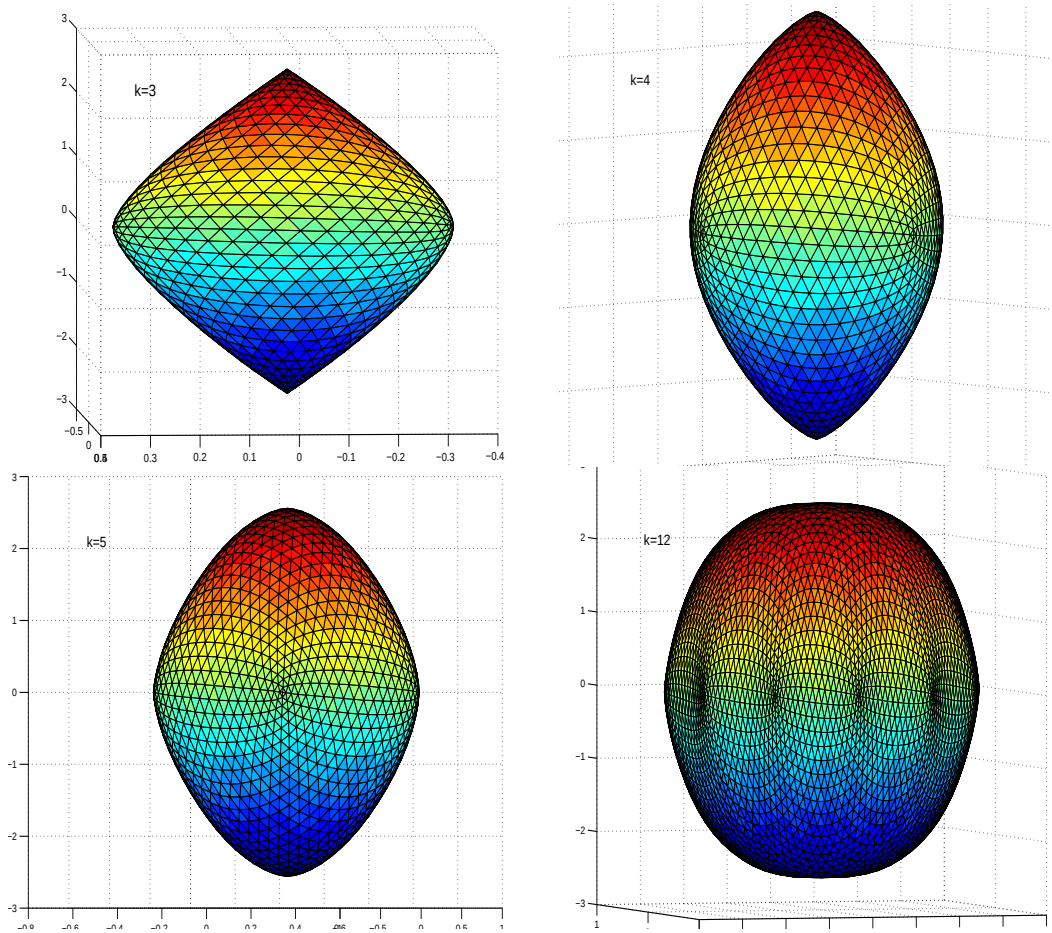


Figure 14: Result after 3 subdivision steps with S from (20) applied to double pyramid over k-gon for $k = 3$, $k = 4$, $k = 5$, and $k = 12$

vertices in this triangulation are regular). This new equation is

$$a' = \frac{85 - 19w}{147} a + \frac{62 + 19w}{147k} \sum_{j=1}^{k} b_j,$$

which has no impact on the definition of $B(z)$ and thus on the eigenvalues of the B_j, $j = 1, \ldots, k-1$. What changes is the first row of B_0, and the parameter w can be used to massage the spectrum of B_0. In particular, the subdominant eigenvalue of B_0 is strictly less than $1/7$ if $0 < w < 2$ (with a minimal value for $w \approx 1.4$) and strictly larger than $1/7$ for $-1 < w < 0$, see Fig. 13 b). Thus, if $k = 3$ we would take $w > 0$ to achieve a pair (instead of a triple) of subdominant, complex-conjugate eigenvalues associated with B_1 and B_2 which is prerequisite for establishing the C^1 property also for extraordinary vertices of valence $k = 3$.

In Figure 15, we show the same double pyramid examples as in Fig. 14, now with the flap modification switched on. The values $w = w(k)$ were chosen ad hoc as $w(3) = 1$, $w(4) = 1/2$, $w(5) = 1/12$, $w(6) = 0$, and $w(12) = -1/2$. Note the considerable im-

provement for $k = 3$ but also a less flat appearance near the pyramid tip for $k = 12$. We caution the reader that these considerations are by no means mathematical statements, however, they may serve as a preliminary assessment of the potential strengths and weaknesses of the proposed scheme. We also mention the potential option of using the parameter w to optimize the local shape of the (discrete) subdivision surface near extraordinary vertices which might be a good idea, especially, in the first few subdivision steps.

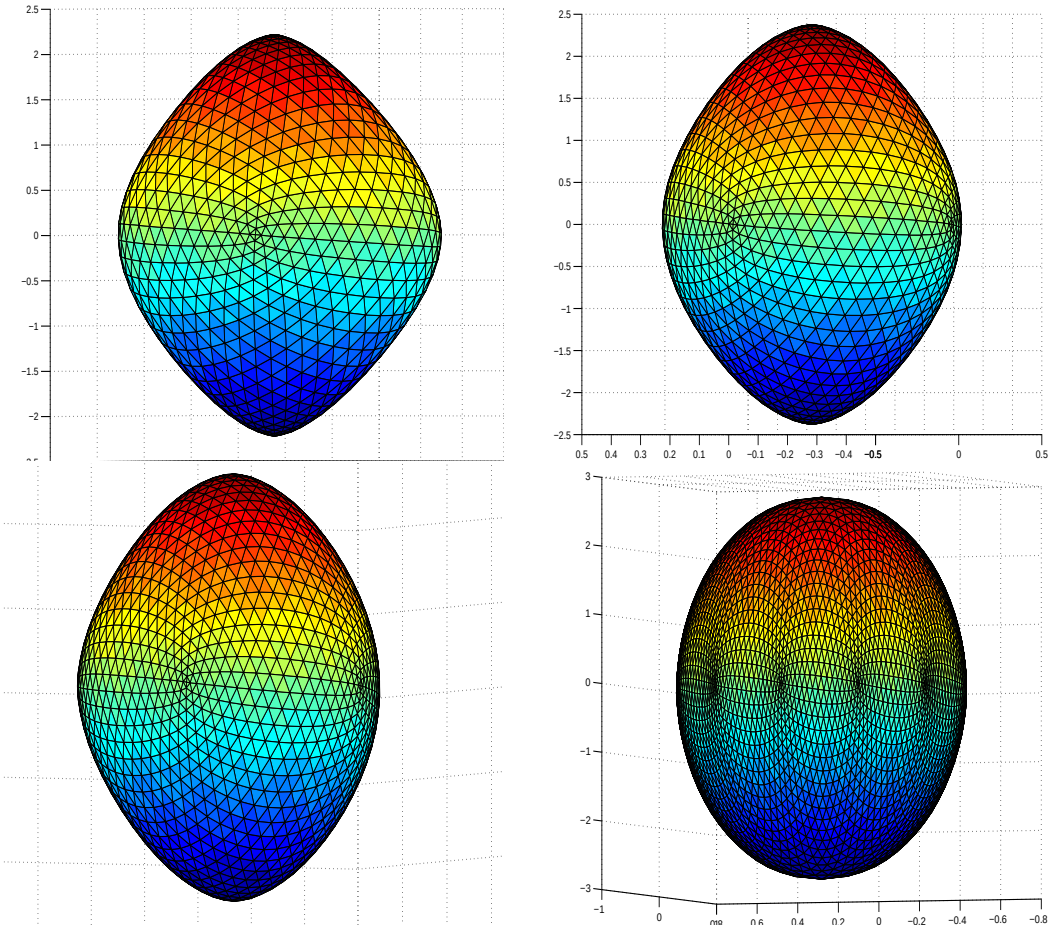


Figure 15: Flap modification, applied to the examples of Fig. 14

E: We briefly mention that the rearrangement

$$\tilde{S} := (\mathcal{F}' \overset{4/7}{\leftarrow} \mathcal{F}' \leftarrow \mathcal{V}') \circ S_{\mathcal{V},lin} \circ (\mathcal{V} \leftarrow \mathcal{F}) \tag{21}$$

of S represents a dual triangular $\sqrt{7}$-scheme, and can be interpreted as primal scheme for polygonal meshes where the valence of all vertices is 3. Since $\sqrt{7}$-refinement of its dual triangular mesh induces only new vertices of valence 6, the refined polygonal meshes predominantly consist of hexagons which will be further split into 7 hexagon. Thus, these schemes are commonly called hex-by-7 schemes. According to Lemma 2,

the scheme $\tilde{S}$ in (21) preserves the smoothness properties of the original scheme S (note that $S' = (\mathcal{F}' \overset{4/7}{\leftarrow} \mathcal{F}' \leftarrow \mathcal{V}') \circ S_{\mathcal{V},lin}$ obviously preserves constants). A drawback is that the sets of refinable functions associated with (21) are not linearly independent. This makes it less obvious how to build multiscale, wavelet-type pyramid algorithms on top of such a subdivision process.

F: In practical geometry applications of subdivision schemes, one would be required to have a way of treating meshes with boundaries. This is a difficult task for the above TR, in particular for its dual, hex-by-7 interpretation. The main obstacle is the constant rotation of the underlying TR. A quick fix is to go back to the suggestion (which we discarded for reasons of simplifying the smoothness analysis) of alternating the orientation of the triangulation. Then, the TR resulting from two subsequent topology refinement steps (with different orientation) corresponds to a standard refinement with $m = 49$, and no rotation. With this in mind one can come up with modifications of the rules near the boundary such that their result (again after two combined steps) is equivalent to a curve subdivision scheme with dilation factor $m = 7$. The same approach has previously been used for $\sqrt{3}$-subdivision schemes [20], where it was managable, mainly because of a smaller dilation factor of $m = 3$ for the resulting curve scheme. Due to the lack of better ideas, we will not further dwell on this issue.

References

[1] M. Botsch, S. Steinberg, S. Bischoff, L. Kobbelt, OpenMesh - a generic and efficient mesh data structure, Preprint, RWTH Aachen, 2003.

[2] A. S. Cavaretta, W. Dahmen, C. A. Micchelli, Stationary subdivision, Memoirs AMS, vol. 93, AMS, Providence, 1991.

[3] J. Claes, K. Beets and F. van Reeth, A corner-cutting scheme for hexagonal subdivision surfaces, Proc. Int. Conf. "Shape Modeling and Applications", Canada, 2002.

[4] N. Dyn, D. Levin, Subdivision schemes in geometric modelling, Acta Numerica 11 (2002), 73–144.

[5] N. A. Dodgson, I. P. Ivrissimtzis, and M. A. Sabin, Characteristics of dual triangular $\sqrt{3}$ subdivision, in Curve and Surface Fitting: Saint Malo 2002, A. Cohen, J.-L. Merrien, L. L. Schumaker (eds.), Nashboro Press, Brentwood, 2003, pp. 119–128.

[6] N. Dyn, D. Levin, J. Simoens, Face value subdivision schemes on triangulations by repeated averaging, in Curve and Surface Fitting: Saint Malo 2002, A. Cohen, J.-L. Merrien, L. L. Schumaker (eds.), Nashboro Press, Brentwood, 2003, pp. 129–138.

[7] B. Han, Computing the smoothness exponent of a symmetric multivariate refinable function, SIAM J. Matr. Anal. Appl., Vol. 24, No. 3 (2003), 693–714.

[8] B. Han, Classification and construction of bivariate subdivision schemes, in Curve and Surface Fitting: Saint Malo 2002, A. Cohen, J.-L. Merrien, L. L. Schumaker (eds.), Nashboro Press, Brentwood, 2003, pp. 187–198.

[9] B. Han, R.-Q. Jia, Multivariate refinement equations and convergence of subdivision schemes, SIAM J. Math. Anal., Vol. 29, No. 5 (1998), 1177–1199.

[10] B. Han, B. Piper, T. P. Yu, Multivariate refinable Hermite interpolants, Mathematics of Computations (2002, to appear).

[11] B. Han, M. L. Overton, and T. P.-Y. Yu, Design of Hermite subdivision schemes aided by spectral radius optimization, SIAM J. Sci. Comp., (2003, to appear).

[12] I. P. Ivrissimtzis, N. A. Dodgson, and M. A. Sabin, A generative classification of mesh refinement rules with lattice transformations, Preprint, Cambridge Univ. 2002.

[13] I. P. Ivrissimtzis, K. Shrivastava, and H.-P. Seidel, Subdivision rules for general meshes, in Curve and Surface Fitting: Saint Malo 2002 A. Cohen, J.-L. Merrien, L. L. Schumaker (eds.), Nashboro Press, Brentwood, 2003, pp. 229–237.

[14] H. Ji, S. D. Riemenschneider, Z. Shen, Multivariate compactly supported fundamental refinable functions, duals, and biorthogonal wavelets, Stud. Appl. Math. 102 (1999), 173–204.

[15] R. Q. Jia, Characterization of smoothness of multivariate refinable functions in Sobolev spaces, Trans. Amer. Math. Soc. 351 (1999), 4089–4112.

[16] R. Q. Jia, Q. Jiang, Spectral analysis of the transition operator and its applications to smoothness analysis of wavelets, SIAM J. Matrix Anal. Appl., to appear.

[17] Q.-R. Jia, S. Zhang, Spectral properties of the transition operator associated to a multivariate refeinement equation, Linear Algebra and its Applications, 292 (1999), 155–178.

[18] Q. Jiang, Multivariate matrix refinable functions with arbitrary matrix dilation, Trans. Amer. Math. Soc. 351 (1999), 2407–2438.

[19] Q. Jiang and P. Oswald, Triangular $\sqrt{3}-$subdivision schemes: The regular case, JCAM 156 (2003), 47–75.

[20] L. Kobbelt, $\sqrt{3}$ subdivision, Proc. SIGGRAPH 2000, 103–112.

[21] M. Kohler, A Meta Scheme for Iterative Refinement of Meshes, Preprint, Uni Dortmund, 1998.

[22] A. Levin, D. Levin, Analysis of quasi-uniform subdivision, ACHA, 15 (2003), 18–32.

[23] C. Loop, Smooth subdivision based on triangular meshes, Master's Thesis, Univ. Utah, Dep. of Mathematics, 1987.

[24] A. Lundmark, N. Wadströmer, H. Li, Hierarchical subsampling giving fractal regions, IEEE Trans. on Image Proc., vol. 10, no. 1, Jan. 2001, 167– 173.

[25] H. Müller, M. Rips, Another Metascheme of Subdivision Surfaces, Research Report no. 713, Uni Dortmund, June 1999.

[26] J. Peters, U. Reif, Analysis of algorithms generalizing B-spline subdivision, SIAM J. Numer. Anal. 35, 2 (1998), 728–748.

[27] P. Oswald, P. Schroeder, Composite primal/dual $\sqrt{3}-$subdivision schemes, CAGD 20, 3 (2003), 135–164.

[28] K. Sahr, D. White, Discrete global grid system, Proc. 30th Symposium on the Interface Computing Science and Statistics 30, 1998, 269–278.

[29] U. Reif, A unified approach to subdivision algorithms near extraordinary points, CAGD 12 (1995), 153–174.

[30] A. Ron, Z. Shen, K. C. Toh, Computing the Sobolev regularity of refinable functions by Arnoldi method, SIAM J. Matrix Anal. Appl., 23 (2001), 57–76.

[31] G. Umlauf, Analyzing the characteristic map of triangular subdivision schemes. Constr. Approx. 16 (2000), 145–155.

[32] A. B. Watson, A. J. Ahumada, Jr., A hexagonal orthogonal-oriented pyramid as a model of image presentation in visual cortex, IEEE Trans. Biomed. Eng. vol. 36, no. 1, Jan. 1989, 97–106.

[33] X. Wu, D. Thompson, R. Machiraju, A generalized corner-cutting subdivision scheme, manuscript, 2002.

[34] D. Zorin, A method for analysis of C^1-continuity of subdivision surfaces, SIAM J. Numer. Anal. 37, 5 (2000), 1677-1708.

[35] D. Zorin, Smoothness of stationary subdivision on irregular meshes, Constr. Approx. 16 (2000), 359–397.